

THE PROPER MOTION OF THE GALACTIC CENTER PULSAR RELATIVE TO SAGITTARIUS A*

GEOFFREY C. BOWER¹, ADAM DELLER², PAUL DEMOREST³, ANDREAS BRUNTHALER⁴, HEINO FALCKE^{5,2,4}, MONIKA MOSCIBRODZKA⁵, RYAN M. O'LEARY⁶, RALPH P. EATOUGH⁴, MICHAEL KRAMER^{4,7}, K.J. LEE⁴, LAURA SPITLER⁴, GREGORY DESVIGNES⁴, ANTHONY P. RUSHTON^{8,9}, SHEPERD DOELEMEN^{10,11}, MARK J. REID¹¹

Draft version March 17, 2016

ABSTRACT

We measure the proper motion of the pulsar PSR J1745-2900 relative to the Galactic Center massive black hole, Sgr A*, using the Very Long Baseline Array (VLBA). The pulsar has a transverse velocity of $236 \pm 11 \text{ km s}^{-1}$ at position angle 22 ± 2 deg East of North at a projected separation of 0.097 pc from Sgr A*. Given the unknown radial velocity, this transverse velocity measurement does not conclusively prove that the pulsar is bound to Sgr A*; however, the probability of chance alignment is very small. We do show that the velocity and position is consistent with a bound orbit originating in the clockwise disk of massive stars orbiting Sgr A* and a natal velocity kick of $\lesssim 500 \text{ km s}^{-1}$. An origin among the isotropic stellar cluster is possible but less probable. If the pulsar remains radio-bright, multi-year astrometry of PSR J1745-2900 can detect its acceleration and determine the full three-dimensional orbit. We also demonstrate that PSR J1745-2900 exhibits the same angular broadening as Sgr A* over a wavelength range of 3.6 cm to 0.7 cm, further confirming that the two sources share the same interstellar scattering properties. Finally, we place the first limits on the presence of a wavelength-dependent shift in the position of Sgr A*, i.e., the core shift, one of the expected properties of optically-thick jet emission. Our results for PSR J1745-2900 support the hypothesis that Galactic Center pulsars will originate from the stellar disk and deepens the mystery regarding the small number of detected Galactic Center pulsars.

Subject headings: pulsars: general, pulsars: individual(PSR J1745-2900), black hole physics, Galaxy: center, proper motions

1. INTRODUCTION

The discovery of the pulsar PSR J1745-2900 at a projected separation of 0.1 pc from the massive black hole in the Galactic Center, Sgr A*, provides an unprecedented opportunity to explore stellar evolution, the population of compact objects, and the interstellar medium of the Galactic Center. Ultimately, these elements contribute to our understanding of the possibility for the use of pulsars in short-period orbits to characterize the space-time metric of the black hole (e.g., Backer & Hellings 1986; Wex et al. 1996; Pfahl & Loeb 2004; Cordes et al. 2004; Liu et al. 2012). In addition, the proximity of the pulsar to Sgr A* provides a unique reference source to characterize the high angular resolution properties of Sgr A* that are obscured by the effects of interstellar scattering (van Langevelde et al. 1992; Frail et al. 1994; Lo et al. 1998; Bower et al. 2004, 2006, 2014b).

PSR J1745-2900 was discovered serendipitously on 24 April 2013 (MJD= 56406) through detection of a strong X-ray burst as part of a daily monitoring campaign carried out by the *Swift* satellite (Kennea et al. 2013). NuSTAR observations then detected periodic flux variations with $P = 3.76$ s and a hydrogen absorption column $N_H \sim 10^{23} \text{ cm}^{-2}$ that is characteristic of a location in the Galactic Center (Mori et al. 2013). *Chandra* observations localized the source offset from Sgr A* by ~ 3 arcseconds, a projected separation of 0.1 pc (Rea et al. 2013). PSR J1745-2900 increased in luminosity by a factor of $\gtrsim 10^3$ over upper limits from deep *Chandra* observations (Muno et al. 2009). The measured period derivative implies a characteristic age of 9 kyr and a magnetic field $\sim 10^{14}$ G, under standard assumptions for magnetic dipole breaking. The transient nature of the X-ray flux and the low spin-down power relative to the X-ray luminosity indicate that PSR J1745-2900 is not a rotation-powered pulsar but a magnetar. Recently, Kaspi et al. (2014) demonstrated a factor of ~ 3 increase in the spin-down rate of the magnetar with hard X-ray observations. The variability of the spin-down rate demonstrates that the characteristic age is accurate to at most an order of magnitude. Association of soft gamma-ray repeaters (SGRs) and anomalous X-ray pulsars (AXPs) with supernova remnants suggests that magnetar ages are $\lesssim 10^4 - 10^5$ yr (Thompson et al. 2002). The instability of the magnetar spin limits the degree to which general relativistic effects can be studied through timing observations.

Pulsed radio emission from PSR J1745-2900 was discovered shortly after the pulsed X-ray emission (Eatough et al. 2013a; Shannon & Johnston 2013). PSR J1745-2900 was found to have the largest dispersion measure, $DM =$

¹ Academia Sinica Institute of Astronomy and Astrophysics, 645 N. A'ohoku Place, Hilo, HI 96720, USA; gbower@asiaa.sinica.edu.tw

² ASTRON, P.O. Box 2, 7990 AA Dwingeloo, The Netherlands

³ NRAO, 520 Edgemont Road, Charlottesville, VA 22903-2475, USA

⁴ Max-Planck-Institut für Radioastronomie, Auf dem Hügel 69, D-53121 Bonn, Germany

⁵ Department of Astrophysics, Institute for Mathematics, Astrophysics and Particle Physics (IMAPP), Radboud University, PO Box 9010, 6500 GL Nijmegen, The Netherlands

⁶ JILA, University of Colorado and NIST, 440 UCB, Boulder, CO 80309-0440, USA

⁷ Jodrell Bank Centre of Astrophysics, University of Manchester, Manchester M13 9PL, UK

⁸ Department of Physics, Astrophysics, University of Oxford, Keble Road, Oxford OX1 3RH, UK

⁹ School of Physics and Astronomy, University of Southampton, Highfield, Southampton SO17 1BJ, UK

¹⁰ MIT Haystack Observatory, Route 40, Westford, MA 01886, USA

¹¹ Harvard-Smithsonian Center for Astrophysics, 60 Garden Street, Cambridge, MA 02138, USA

$1778 \pm 3 \text{ pc cm}^{-3}$, and rotation measure, $RM = -66960 \pm 50 \text{ rad m}^{-2}$, of any known pulsar. These large values are consistent with the source being embedded in the dense, magnetized plasma of the Galactic Center. High resolution very long baseline interferometry (VLBI) demonstrated that the pulsar also shares the extreme angular broadening of Sgr A* (Bower et al. 2014a). Pulsar timing show that the pulse width scales as ν^4 and that pulses can be detected to frequencies below 2 GHz (Spitler et al. 2014). Three other pulsars in the central 40 pc of the Galaxy show temporal broadening that is comparable to that of PSR J1745-2900 i.e., $\sim 1 \text{ sec}$ at 1 GHz (Johnston et al. 2006; Deneva et al. 2009). Using the model of a geometrically thin scattering screen in combination with angular and temporal broadening, Bower et al. (2014a) demonstrate that a substantial fraction of the scattering must occur at distances of kiloparsecs away from the Galactic Center; alternate explanations that lead to large temporal scattering may still be found (Spitler et al. 2014).

If the scattering screen is in fact distant from the Galactic Center as the most straight-forward interpretation suggests, then the shared scattering properties of PSR J1745-2900 and Sgr A*, and the detection of radio pulses at frequencies as low as 1.6 GHz indicate that pulsars bound to Sgr A* and, likely, throughout the Galactic Center can be readily detected. Strikingly, such pulsars have not been found in targeted radio searches over a wide range of frequencies (e.g., Kramer et al. 2000; Johnston et al. 2006; Deneva et al. 2009; Macquart et al. 2010; Siemion et al. 2013; Eatough et al. 2013b). Previously, the absence of Galactic Center pulsars was attributed to extreme temporal broadening at low radio frequencies and the steep spectra of radio pulsars. Theory, however, has predicted populations hundreds to thousands of pulsars bound to Sgr A* based on the high rate of star formation and the large massive star population (e.g., Pfahl & Loeb 2004; Freitag et al. 2006; Wharton et al. 2012; Zhang et al. 2014). The massive stars may have produced ~ 20 pulsar wind nebulae in the central 20 pc, as seen through extended X-ray emission (Muno et al. 2008). Finally, while pulsars have not been discovered, a dense cluster of compact objects within the central parsec, many known to be black hole binaries, has been detected through transient X-ray and radio emission (Muno et al. 2005; Bower et al. 2005).

The absence of pulsar discovery has raised the issue of whether there is a problem of missing pulsars in the Galactic Center. This has led to discussion of alternative pulsar populations in the Galactic Center. Dexter & O’Leary (2014) argue that the detection of a rare radio magnetar and the demonstration of the ability to detect ordinary pulsars implies that the pulsar population of the Galactic Center may be distinct from the field population. Bramante & Linden (2014) argue that dark matter could interact with neutron stars and lead them to collapse into black holes. Ultimately, deeper surveys will be required to determine whether the population is truly peculiar (Chennamangalam & Lorimer 2014).

In this paper, we measure the astrometric properties of the pulsar PSR J1745-2900. The proper motion and acceleration provide important constraints on the origin of the pulsar. In particular, we explore whether the pulsar has originated in the Galactic Center cluster stellar disk, which theory has predicted as the origin for the bulk of the pulsar population. In addition, the proper motion can be used to translate time-domain variations in the propagation quantities (DM, RM, angular broadening, temporal broadening) into linear units. This will provide a powerful probe of the length-scale of turbulent properties in the Galactic Center.

Simultaneously, we use astrometric measurements of PSR J1745-2900 relative to Sgr A* to constrain the radiative properties of Sgr A*. Sgr A* shows some of the most extreme scattering properties of any radio source with an angular size of $\sim 0.5 \text{ arcsec}$ at 21 cm and scaling with λ^2 (Bower et al. 2004, 2006, 2014b). The angular broadening obscures the underlying physical processes such that we are not able to determine whether a jet or accretion disk is responsible for the nonthermal emission. Our new observations provide the most accurate measurements of the size of Sgr A* at wavelengths of 2.0 and 3.5 cm. In addition, jet theory predicts that the core of the radio emission will shift as a function of wavelength due to differences in the opacity (Blandford & Konigl 1979; Falcke 1999). This “core shift” has been seen in other radio sources powered by jets, most notably M81 and M87 (Bietenholz et al. 2004; Hada et al. 2011). Our phased-reference measurement of the position of PSR J1745-2900, which is intrinsically point-like with a position independent of wavelength, therefore, provides a unique probe of the wavelength-dependent structure of the reference source, Sgr A*. These observations are complementary to short wavelength VLBI observations ($\lambda \gtrsim 1.3 \text{ mm}$; Doeleman et al. 2008; Fish et al. 2011) which will image the inner accretion disk and/or the base of the jet, and explore smaller-scale frequency-dependent general relativistic effects (Broderick & Loeb 2006).

In Section 2 we present our Very Long Baseline Array (VLBA) observations spanning the first year since the discovery of the pulsar. In Section 3, we discuss results for the motion and origin of the pulsar and conclude that it is likely that the pulsar originated in the stellar disk. In Section 4, we present results on the angular broadening and core shift. We provide our conclusions in Section 5.

2. OBSERVATIONS AND DATA REDUCTION

The observing setup was already described in detail in Bower et al. (2014a); we briefly summarize it here. Observations were 6 hours in duration, taken under the VLBA project codes BB336, BB337 and BB339. Pulsar gating was used with a pulse width that varied between observations due to the changing magnetar pulse profile. A gate stretching from the $\sim 10\%$ point at the rising edge of the pulse to the $\sim 10\%$ point at the trailing edge of the pulse was applied, with a total duration of 100-300 ms. At 8 GHz and above, the scattering time is far shorter than the intrinsic pulse width ($\leq 1 \text{ ms}$; Spitler et al. 2014), so virtually all of the scattered emission is captured. After the observations already presented in Bower et al. (2014a), we began observing at both Ku band (15.3 GHz) and X band (8.6 GHz) within a single observation, changing frequencies on a timescale of 8 minutes. In addition, one observation of Sgr A* at higher frequencies (22 GHz and 43 GHz; project code BR187) without the VLA was included. For the observations

TABLE 1
 OBSERVATIONS OF PSR J1745-2900

Epoch (MJD)	Observing band	Observing frequency (GHz)	BR	FD	KP	LA	NL	OV	PT	Y ^A
56422	X	8.540 – 8.796	✓	✓	✓	✓	✓	✓	✓	D
56444	X	8.540 – 8.796	✓	✓	✓ ^B	✓ ^B	✓	✓	✓	C ^C
56473	Ku	15.240 – 15.496	✓	...	✓	✓	✓	✓	✓	C
56486	X	8.540 – 8.796	✓	...	✓	✓	✓	✓	✓	C
56556	X, Ku	8.540 – 8.796, 15.240 – 15.496	✓	✓	✓	✓	✓	B
56658	X, Ku	8.540 – 8.796, 15.240 – 15.496	✓	✓	...	✓	✓	✓	✓	BnA
56710	X, Ku	8.540 – 8.796, 15.240 – 15.496	✓	✓	...	✓	✓	✓	✓	A
56750	K, Q,	21.792 – 22.048, 42.768 – 43.024	✓	✓	✓	✓	...	✓	✓	...
56772	X, Ku	8.540 – 8.796, 15.240 – 15.496	✓	...	✓	✓	...	✓	✓	A
56892	Ku, Q	15.240 – 15.496, 43.168 – 43.424	✓	✓	✓	✓	✓	✓	✓	D ^D
56899	K, Q,	21.792 – 22.048, 42.768 – 43.024	✓	✓	✓	✓	✓	✓	✓	...

^A Denotes the VLA configuration for the phased-array observation.

^B Disk pack problems resulted in the loss of 25% of the data from this station.

^C Problems with the array phasing resulted in the loss of 35% of the VLA data from this epoch.

^D Atmospheric turbulence at the VLA caused array phasing at Q band to fail.

of MJD 56556 onwards, we used Sgr A* as the reference source for phasing the VLA, eliminating the need to slew to an external calibrator. One epoch (MJD 56556) failed due to the absence of two of the critical southwestern antennas. Table 1 summarizes the observing dates, frequencies, and participating antennas.

At all frequencies, a simple Gaussian model of Sgr A* with the size predicted by Bower et al. (2006) was used as a starting model for the highest-quality epoch at that frequency. After initial calibration, we concatenated data from all epochs for the Sgr A* field (separately for each frequency band) and iteratively imaged and self-calibrated the combined datasets to generate high-quality clean component models. These clean component models (1 per frequency) were subsequently used for all observations at that frequency, with the position adjusted to the expected position of Sgr A* at that epoch based on the fit of Reid & Brunthaler (2004). These models were adjusted to the new and more accurate closure amplitude fits at these wavelengths for Sgr A* obtained below. Closure amplitudes were not used for the pulsar size because of the low SNR for the pulsar. In this way, the residual delay rates due to geometric model errors were minimised, and we obtain positions for Sgr A* and PSR J1745-2900 which are approximately correct in the International Celestial Reference Frame (ICRF), with an absolutely positional uncertainty of ~ 10 milliarcseconds due to the reference position and proper motion uncertainty of Sgr A* as given by Reid & Brunthaler (2004). The assumed proper motion of Sgr A* is $\mu_{SgrA*} = (-3.151, -5.547)$ mas yr⁻¹ with position (17:45:40.0366, -29:00:28.217) at epoch MJD=56710.

After calibration, we performed for all epochs a visibility-by-visibility subtraction of the ungated dataset from the gated dataset as described in Bower et al. (2014a) to remove the effect of Sgr A* from the image of PSR J1745-2900. A Gaussian model fit was performed in the visibility domain with the `difmap` package (Shepherd 1997), and errors on the size and position were estimated using the image-plane fitting task `JMFIT` in AIPS (Greisen 2003). In all cases, the best `modelfit` result from `difmap` was consistent with the image-plane fit from `JMFIT` to within the errors. We use the `JMFIT` results and errors in the analysis below. Table 2 shows the flux densities and observed positions for each epoch and band.

Table 3 reports measured apparent sizes for PSR J1745-2900 and Sgr A*. Apparent sizes for PSR J1745-2900 were determined from image fits as described above with deconvolution of the synthesized beam. Sizes for Sgr A* were determined from closure amplitude fitting following the techniques described in (Bower et al. 2014b). These provide the highest quality measurements of the size of Sgr A* at these wavelengths.

3. ASTROMETRIC RESULTS FOR PSR J1745-2900

We show positions as a function of time in Figure 1. We fit the proper motion, acceleration, and core shift to the astrometric position of PSR J1745-2900 using the following equations:

$$\begin{aligned} \Delta\alpha &= \Delta\alpha_0 + \mu_\alpha * (\text{MJD} - \text{MJD}_0) + \frac{1}{2}a_\alpha * (\text{MJD} - \text{MJD}_0)^2 - \Phi_\alpha\lambda \\ \Delta\delta &= \Delta\delta_0 + \mu_\delta * (\text{MJD} - \text{MJD}_0) + \frac{1}{2}a_\delta * (\text{MJD} - \text{MJD}_0)^2 - \Phi_\delta\lambda, \end{aligned} \quad (1)$$

where $\text{MJD}_0 = 56686$ is the mid-point of our observations. Solutions are calculated for proper motion only ($a = 0, \Phi = 0$), proper motion and acceleration ($\Phi = 0$), and proper motion and core shift ($a = 0$). Results are tabulated in Table 4. Note that the sign on the final term is defined to reflect that the core shift is reflective of an actual shift in the position in Sgr A*. Fits were performed using a weighted least-squares method for each solution with errors for each data point rescaled such that the reduced χ^2 was equal to one.

3.1. Astrometric Error Analysis

TABLE 2
OBSERVED POSITIONS OF PSR J1745-2900

MJD	Band	Flux Density (mJy)	ICRF RA (J2000)	ICRF Dec. (J2000)	$\Delta\alpha$ (mas)	$\Delta\delta$ (mas)
56422	X	0.56	17 45 40.166377 \pm 0.000020	-29 00 29.8960 \pm 00.0002	1699.97 \pm 0.26	-1683.38 \pm 0.20
56444	X	0.76	17 45 40.166327 \pm 0.000012	-29 00 29.8962 \pm 00.0001	1699.50 \pm 0.16	-1683.24 \pm 0.10
56473	Ku	0.58	17 45 40.166263 \pm 0.000008	-29 00 29.8962 \pm 00.0001	1698.91 \pm 0.10	-1682.80 \pm 0.10
56486	X	1.47	17 45 40.166222 \pm 0.000008	-29 00 29.8965 \pm 00.0001	1698.49 \pm 0.10	-1682.90 \pm 0.10
56658	Ku	2.09	17 45 40.166264 \pm 0.000007	-29 00 29.8960 \pm 00.0001	1700.52 \pm 0.09	-1679.79 \pm 0.10
...	X	1.18	17 45 40.166276 \pm 0.000010	-29 00 29.8960 \pm 00.0001	1700.68 \pm 0.13	-1679.79 \pm 0.10
56710	Ku	1.07	17 45 40.166249 \pm 0.000005	-29 00 29.8960 \pm 00.0001	1700.77 \pm 0.07	-1679.00 \pm 0.10
...	X	0.94	17 45 40.166237 \pm 0.000014	-29 00 29.8962 \pm 00.0002	1700.62 \pm 0.18	-1679.20 \pm 0.20
56750	K	0.92	17 45 40.166235 \pm 0.000004	-29 00 29.8961 \pm 00.0001	1700.94 \pm 0.05	-1678.49 \pm 0.10
...	Q	0.54	17 45 40.166238 \pm 0.000003	-29 00 29.8959 \pm 00.0001	1700.98 \pm 0.04	-1678.29 \pm 0.10
56772	X	1.00	17 45 40.166246 \pm 0.000016	-29 00 29.8958 \pm 00.0002	1701.27 \pm 0.21	-1677.86 \pm 0.20
...	Ku	1.22	17 45 40.166204 \pm 0.000008	-29 00 29.8961 \pm 00.0001	1700.72 \pm 0.10	-1678.16 \pm 0.10
56892	Ku	0.63	17 45 40.166196 \pm 0.000028	-29 00 29.8959 \pm 00.0003	1701.65 \pm 0.37	-1676.15 \pm 0.30
56899	K	0.26	17 45 40.166250 \pm 0.000025	-29 00 29.8959 \pm 00.0003	1702.42 \pm 0.33	-1676.06 \pm 0.30
...	Q	0.15	17 45 40.166215 \pm 0.000005	-29 00 29.8958 \pm 00.0001	1701.95 \pm 0.07	-1675.90 \pm 0.10

TABLE 3
APPARENT SIZES OF PSR J1745-2900 AND SGR A*

MJD	Band	PSR J1745-2900			Sgr A*		
		b_{maj} (mas)	b_{min} (mas)	b_{pa} (deg)	b_{maj} (mas)	b_{min} (mas)	b_{pa} (deg)
56422	X	16.9 ^{+0.9} _{-0.9}	9.1 ^{+1.2} _{-1.3}	81.4 ^{+6.3} _{-5.9}	17.24 ^{+0.05} _{-0.07}	9.00 ^{+0.32} _{-0.40}	82.0 ^{+0.9} _{-0.7}
56444	X	15.0 ^{+0.6} _{-0.6}	5.2 ^{+1.2} _{-1.4}	88.8 ^{+3.7} _{-3.4}	16.92 ^{+0.20} _{-0.20}	8.40 ^{+0.56} _{-0.52}	81.6 ^{+1.9} _{-1.2}
56473	Ku	5.4 ^{+0.5} _{-0.5}	2.3 ^{+1.0} _{-2.0}	78.2 ^{+9.8} _{-9.2}	5.42 ^{+0.02} _{-0.02}	2.87 ^{+0.04} _{-0.14}	81.8 ^{+0.4} _{-0.4}
56486	X	15.2 ^{+0.3} _{-0.3}	8.5 ^{+0.5} _{-0.5}	78.2 ^{+3.0} _{-2.5}	16.88 ^{+0.17} _{-0.16}	8.04 ^{+1.00} _{-0.68}	81.2 ^{+2.9} _{-1.9}
56658	Ku	4.9 ^{+0.6} _{-0.5}	3.0 ^{+1.1} _{-1.7}	78.2 ^{+17.3} _{-15.7}	5.38 ^{+0.07} _{-0.03}	2.52 ^{+0.07} _{-0.08}	81.8 ^{+1.0} _{-1.2}
...	X	16.3 ^{+0.7} _{-0.7}	8.5 ^{+1.1} _{-1.3}	82.1 ^{+4.8} _{-4.4}	16.88 ^{+0.31} _{-0.29}	8.64 ^{+0.64} _{-0.60}	86.4 ^{+1.2} _{-2.4}
56710	Ku	5.0 ^{+0.3} _{-0.3}	2.1 ^{+0.7} _{-1.1}	84.2 ^{+5.9} _{-6.7}	5.43 ^{+0.01} _{-0.12}	2.70 ^{+0.09} _{-0.10}	81.8 ^{+0.4} _{-0.2}
...	X	17.2 ^{+0.6} _{-0.6}	8.0 ^{+0.9} _{-0.9}	84.3 ^{+3.5} _{-3.2}	17.04 ^{+0.12} _{-0.12}	8.04 ^{+0.44} _{-0.48}	81.6 ^{+0.7} _{-0.4}
56750	K	2.6 ^{+0.3} _{-0.2}	1.4 ^{+0.5} _{-0.9}	86.5 ^{+14.0} _{-12.2}	2.68 ^{+0.00} _{-0.00}	1.45 ^{+0.03} _{-0.03}	81.8 ^{+0.0} _{-0.0}
...	Q	0.5 ^{+0.2} _{-0.5}	0.3 ^{+0.6} _{-0.3}	98.3 ^{+40.4} _{-41.2}	0.730 ^{+0.003} _{-0.001}	0.41 ^{+0.02} _{-0.01}	80.0 ^{+0.6} _{-1.2}
56772	X	15.4 ^{+0.9} _{-0.5}	9.9 ^{+0.8} _{-1.5}	80.1 ^{+5.2} _{-10.6}	17.00 ^{+0.11} _{-0.11}	8.28 ^{+0.68} _{-0.64}	81.6 ^{+0.8} _{-0.5}
...	Ku	5.5 ^{+0.5} _{-0.5}	3.6 ^{+0.8} _{-1.0}	78.9 ^{+12.8} _{-13.1}	5.38 ^{+0.02} _{-0.02}	2.71 ^{+0.10} _{-0.13}	81.8 ^{+0.2} _{-0.4}
56892	Ku	7.0 ^{+1.9} _{-2.1}	2.3 ^{+3.1} _{-2.3}	77.0 ^{+28.0} _{-24.0}	5.41 ^{+0.01} _{-0.01}	2.71 ^{+0.07} _{-0.07}	81.8 ^{+0.2} _{-0.2}
56899	K	3.6 ^{+1.1} _{-3.6}	4.0 ^{+0.1} _{-4.0}	95.0 ^{+15.0} _{-37.0}	2.84 ^{+0.02} _{-0.02}	2.16 ^{+0.01} _{-0.12}	94.4 ^{+2.4} _{-2.4}
...	Q	< 0.7	0.722 ^{+0.005} _{-0.003}	0.14 ^{+0.06} _{-0.04}	87.2 ^{+0.6} _{-1.2}
Avg.	X	15.6 ^{+1.3} _{-0.4}	8.4 ^{+0.8} _{-1.7}	82.5 ^{+4.5} _{-3.5}	17.16 ^{+0.05} _{-0.05}	8.64 ^{+0.28} _{-0.28}	82.0 ^{+0.7} _{-0.5}
Avg.	Ku	5.2 ^{+0.4} _{-0.2}	2.8 ^{+0.7} _{-0.6}	81.4 ^{+2.8} _{-3.2}	5.41 ^{+0.01} _{-0.01}	2.62 ^{+0.05} _{-0.05}	81.8 ^{+0.2} _{-0.2}
Avg.	K	2.6 ^{+1.0} _{-0.1}	1.7 ^{+2.3} _{-0.3}	88.2 ^{+6.8} _{-1.7}	2.70 ^{+0.01} _{-0.01}	1.58 ^{+0.06} _{-0.06}	83.6 ^{+0.6} _{-0.6}
Avg.	Q	0.6 ^{+0.1} _{-0.1}	0.0 ^{+0.3} _{-0.0}	96.9 ^{+1.7} _{-6.9}	0.730 ^{+0.003} _{-0.003}	0.36 ^{+0.03} _{-0.01}	81.8 ^{+0.6} _{-1.2}

As shown in Table 4, inclusion of constant acceleration (due to Sgr A*) and/or constant core shift terms do not return detections of either of those parameters or significantly alter the quality of the fits. Accordingly, we consider here the proper-motion-only fits in order to assess the presence of systematic errors in our measured PSR J1745-2900 positions. Using all of the data and the formal positional errors estimated from JMFIT, we calculate χ^2 values for each fit in right ascension and declination. None of the χ^2 values are consistent with a good fit and accurately estimated errors. In particular, errors in declination are underestimated by \sim 25% while errors in right ascension are underestimated by a factor of \sim 3. As shown in Figure 1, there is an apparent systematic error in the right ascension position associated with the first four epochs which accounts for most of the increase in χ^2 . A number of potential effects could cause this discrepancy, and we examine each of them in turn.

The first three possibilities concern calibration. As noted in Bower et al. (2014b), it is difficult to generate an accurate model of Sgr A* to use for calibration, because scatter-broadening causes it to be heavily resolved on most VLBA baselines. This problem is doubly severe in right ascension compared to declination, as the shorter VLBA baselines are predominantly east-west (meaning higher resolution in the right ascension coordinate) and the major axis of Sgr A* scattering is almost aligned with the right ascension axis. An incorrect model of Sgr A* will lead to different positional offsets between epochs if the (u, v) coverage differs (which it does, due to different failed antennas), as the calibration changes the data in order to match the incorrect model. In this sense the first 4 epochs are not

TABLE 4
 PROPER MOTION FITS FOR PSR J1745-2900

Parameter	Units	PM Bootstrap	PM LSQ	PM + Accel.	PM + Core Shift
$\Delta\alpha_0$	(mas)	1700.53 ± 0.07	1700.52 ± 0.07	1700.54 ± 0.09	1700.52 ± 0.19
$\Delta\delta_0$	(mas)	-1679.41 ± 0.03	-1679.41 ± 0.03	-1679.42 ± 0.05	-1679.35 ± 0.10
μ_α	(mas/yr)	2.45 ± 0.33	2.50 ± 0.22	2.49 ± 0.23	2.51 ± 0.31
μ_δ	(mas/yr)	5.88 ± 0.11	5.90 ± 0.09	5.92 ± 0.10	5.84 ± 0.12
a_α	(mas/yr ²)	-0.2 ± 1.0	...
a_δ	(mas/yr ²)	0.2 ± 0.5	...
Φ_α	(mas/cm)	-0.00 ± 0.10
Φ_δ	(mas/cm)	0.03 ± 0.05
$\chi^2_{\alpha}/d.o.f._{\alpha}$	112.3/13	111.8/12	112.3/12
$\chi^2_{\delta}/d.o.f._{\delta}$	17.0/13	16.8/12	16.5/12

especially poor, nor should this type of error lead to a right ascension error which apparently varies linearly with time. It would affect the 8 GHz observations more severely than 15 GHz due to the more severe effects of scattering, and a higher proportion of the first four epochs are at 8 GHz, so this could simply be random errors giving the appearance of linear motion in the first four epochs.

Second, the calibration of the phased VLA could be worse in the first 4 epochs. During this time, we used the source NRAO 530 to determine the real-time solutions to phase up the VLA, and after this time we used Sgr A* itself. The angular offset from our target field to NRAO 530 is 16 deg, and so it is likely that the phased VLA gain is slightly lower and more time variable in these epochs. Since the VLA heavily affects the calibration solution, being the most sensitive antenna, errors in its gain calibration could propagate through to larger errors in the other telescopes gain calibrations and hence positional offsets. There is a direct link to the first 4 epochs, however, there is once again no reason to expect an apparently linear motion with time.

Third, ionospheric effects can introduce wavelength dependent astrometric errors. In the case of our experiment, the small separation, δr , between calibrator and target leads to a correspondingly small error in relative positions (Reid & Honma 2014). After the application of total electron content (TEC) models as part of our calibration, residual ionospheric delay could correspond to $\lesssim 10$ cm at 3.5 cm. This corresponds to an error of ~ 3 beamwidths, or $\delta\theta \lesssim 10$ mas at 3.5 cm. This leads to an astrometric error for the 3.5 cm relative to a shorter wavelength (e.g., 7 mm) position where ionospheric effects are very small of $\delta r \delta\theta \lesssim 1 \mu\text{as}$. Thus, ionospheric effects do not affect our result.

Fourth, the apparent structure of Sgr A* itself could change with time. Since we use a constant model at each frequency (derived from the concatenated datasets at that frequency) there is no way to detect or account for such a change, which could be due to intrinsic source effects (such as a time-variable core shift due to material propagating outwards along a jet) or time-variable scattering or scintillation. By forcing Sgr A* back to the model position during calibration, we would impose an equivalent shift on the target magnetar. Unlike the previous two explanations, evolution of Sgr A* could lead to a linear position change with time, and it would likely be along the right ascension axis, which is both the major axis for the scattering and for the intrinsic structure of Sgr A*. However, the effect we see seems too large for this to be a likely explanation. Various estimates of the scatter-broadened size of Sgr A* (Bower et al. 2006, 2014b) show it to be constant over time within the error bars, and the intrinsic size of Sgr A* is likely much smaller than the required shifts here. The specific case of a time-variable core shift is considered in more detail in Section 4.

Fifth, refractive wander could induce variations in the position of the size on an angular scale smaller than the size of the scattered image. The motion of ~ 1 mas in right ascension is much less than the image size of ~ 15 mas. The short timescale of the fluctuation $\sim 10^2$ days, however, appears inconsistent with the refractive timescale $\tau_R \sim D\theta/v \gtrsim 8 \times 10^2$ days at 3.4 cm, where $D \sim 3$ kpc is the Earth to scattering screen distance, θ is the scatter-broadened angular size, and $v \sim 100\text{km s}^{-1}$ is the relative velocity of the screen perpendicular to the line of sight. τ_R is a minimum timescale for significant refractive changes because the turbulent medium may be uniform on scales larger than $D\theta$ in the scattering screen. As noted above, the apparent size of Sgr A* has remained constant over the course of $\gtrsim 10$ yr, suggesting that the refractive timescale is likely quite large. In addition, the similarity between the pulsar and Sgr A* images, discussed below, suggests that the timescale for refractive changes could be as large as $R/v \approx 1000$ yr, where $R \sim 0.1$ pc is the separation between the two sources. Further, previous attempts to detect positional wander in Sgr A* relative to background quasars at a separation of 0.5 deg have not shown any effect on scales larger than 400 μas on time scales ranging from ~ 1 hour to 1 month (Reid et al. 2008). Longer timescales were probed by observations of water masers in Sgr B2, which has a similar degree of scatter broadening to Sgr A* (Gwinn et al. 1988). No positional wander was detected on a timescale of 6 months to a limit of 18 μas rms for maser spots spread over a region 4'' in scale.

On the other hand, the astrometric offsets we see are only a fraction of the total potential refractive image wander, and thus could potentially occur on (proportionately) shorter timescales than τ_R . In particular, the recent discovery of substructure in the image of Sgr A* at 1.3 cm wavelength (Gwinn et al. 2014) suggests that refractive effects could impact the determination of the centroid of PSR J1745-2900 and the correct model for Sgr A*. Point-like emission with a flux density $\sim 1\%$ of the total flux density was found, effectively demonstrating that Sgr A* resides in the

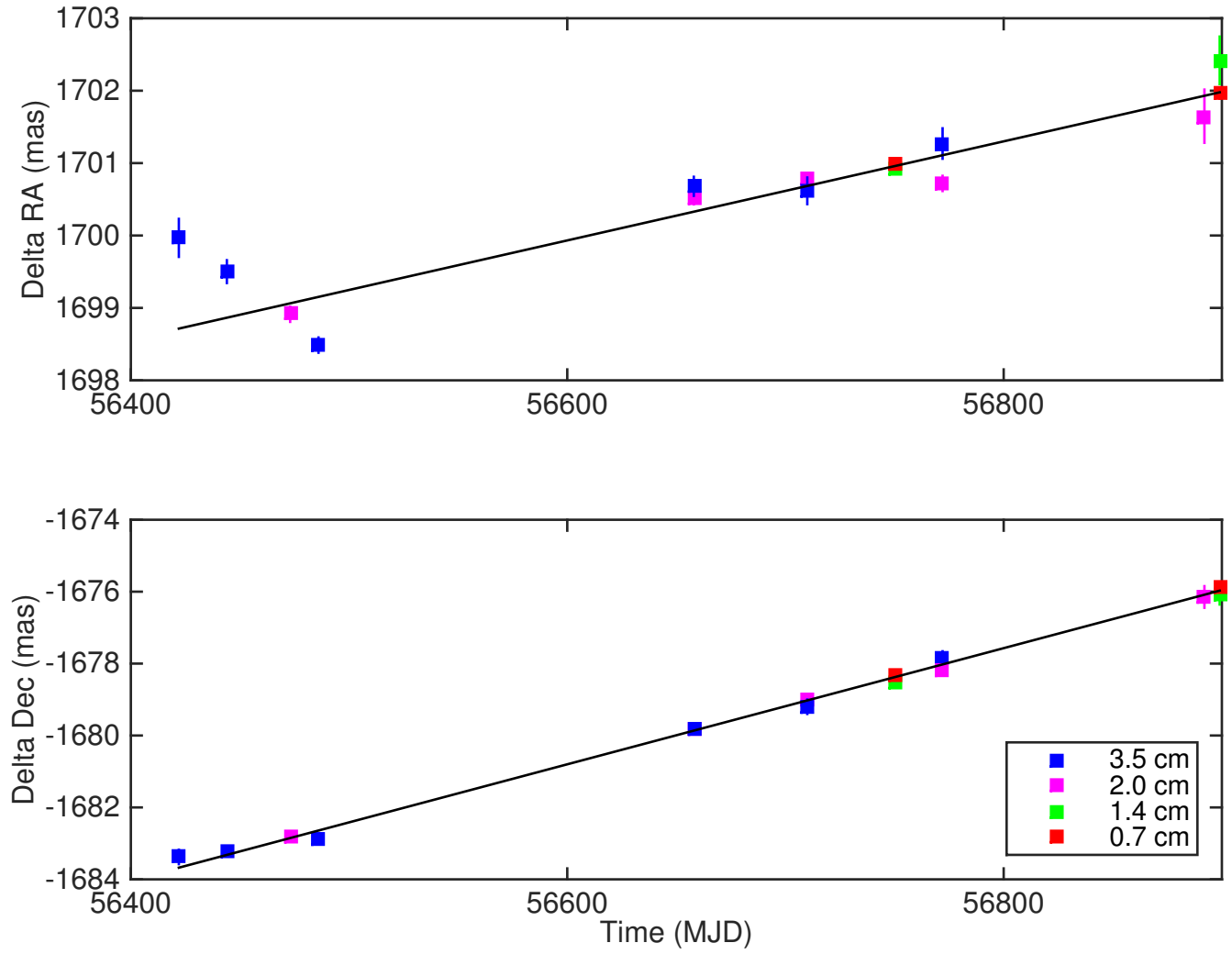


FIG. 1.— Position as a function of time for PSR J1745-2900 relative to Sgr A*. Different colors are used to identify the wavelength of observations. The solid black line shows the best-fit proper motion in each coordinate (see text for details of the fit).

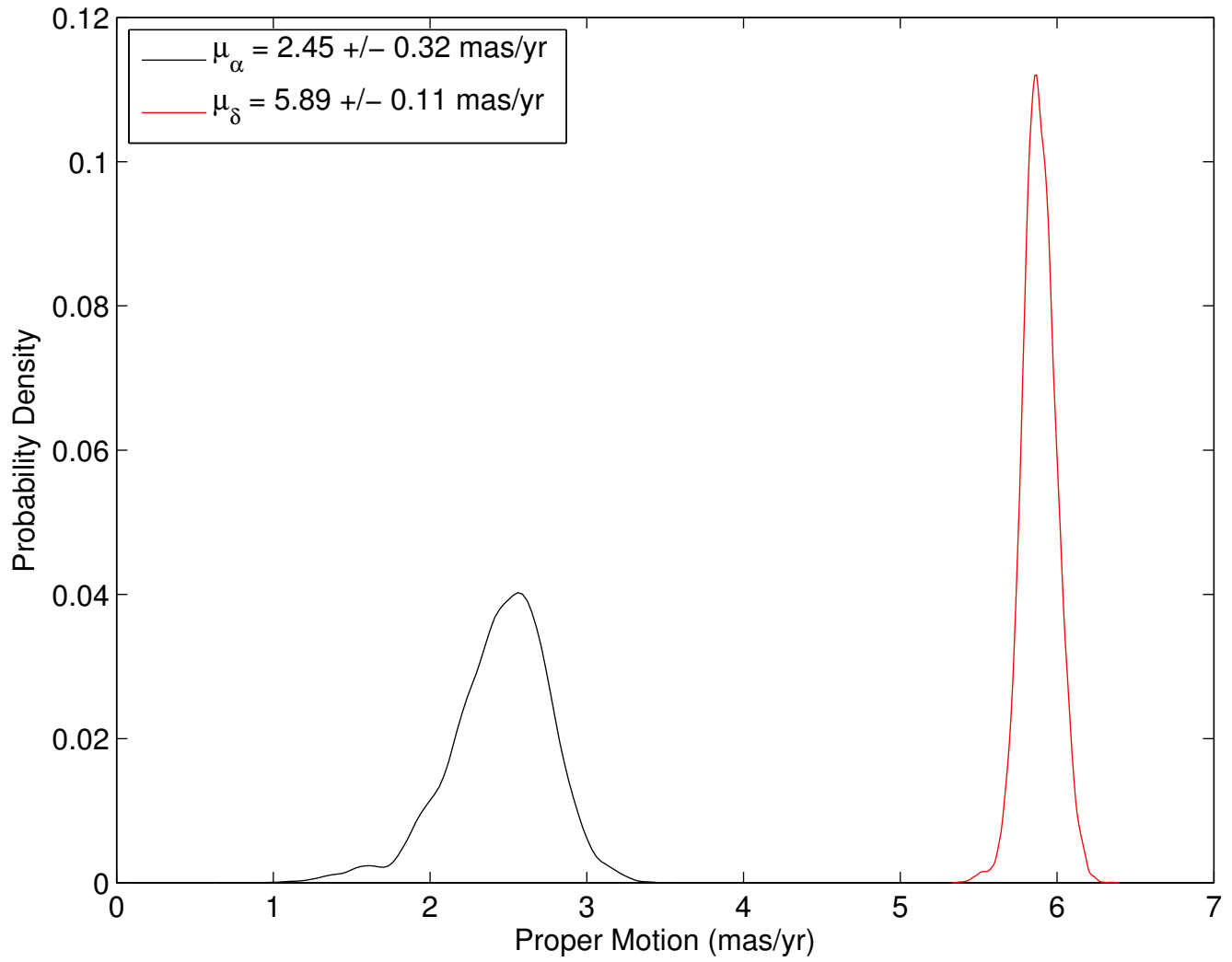


FIG. 2.— Empirical probability density distribution of proper motion solutions from the bootstrap resampling method.

“average” image regime (Narayan & Goodman 1989; Goodman & Narayan 1989). The characteristic time scale for the average image regime ranges from the diffractive timescale ~ 1 sec to the time for an interferometric resolution element to move by a single beam ~ 10 yr, i.e., comparable to the refractive timescale. The amplitude of refractive image wander relative to the scattered size in the case of a shallow turbulent spectrum ($\alpha < 2$) will scale as the ratio of the substructure to peak flux densities. That ratio is ~ 100 at 1.3 cm in the results from Gwinn et al. (2014), a factor of 10 smaller than the actual imaging errors at 3.4 and 2.0 cm. Steeper turbulent spectra can lead to more widely varying refractive image wander. We also do not know whether refractive image wander would be independent between Sgr A* and PSR J1745-2900 if the image wander is common between the two sources then there would be no astrometric effect in our data. For a single epoch of our data at Ku band, we did fit a Gaussian scattering model plus point source and found no significant change in the resultant position for PSR J1745-2900. More detailed study of the wavelength characteristics and time variability of this substructure can determine whether refractive image wander is a significant limitation for astrometry of PSR J1745-2900.

Finally, the change in proper motion in right ascension could be due to real acceleration of the magnetar, during a close encounter with a massive star (a wide companion in a highly elliptical orbit, or a chance encounter). To produce the apparent change in proper motion between the first four and the last four epochs would require acceleration $\sim 1.5 \text{ cm s}^{-2}$, equivalent to the effect of a massive star at a distance $\sim 10^{-3}$ pc, or 25 mas. No star is known to be this close to PSR J1745-2900 (see the discussion below). We also consider this implausible, since the radial acceleration from such an encounter would also affect the pulsar timing, and no large deviations from the long-term timing trends are seen around MJD 56500. In particular, for an edge-on orbit we require a change in the period derivative of $\sim 10^{-10}$, an order of magnitude larger than the period derivative $\dot{P} = 6.12 \times 10^{-12}$ measured by Kaspi et al. (2014) at this epoch. In fact, timing observations detected an abrupt change in the period derivative at MJD=56450, in the middle of the apparently linear proper motion and, therefore, in conflict with orbital motion. If we take the conservative estimate of the measured period derivative as entirely due to acceleration, we set an upper limit that the inclination angle must be $\lesssim 4$ deg. A more detailed analysis of the timing data will set even stronger constraints. Thus, the encounter would have to had been seen almost face on, an unlikely but not impossible scenario.

Ultimately, we cannot confirm or rule out any of the explanations listed above with the exception of differential ionospheric errors. Additional astrometric epochs may eventually provide enough information to favour one of these explanations, but the additional uncertainty imposed on the right ascension proper motion due to the scatter in the first four epochs does not alter any of the conclusions which follow in this paper. Removing this systematic uncertainty and approaching the S/N limited uncertainty in proper motion, however, will be crucial in detecting the acceleration of PSR J1745-2900 due to Sgr A* over a long period (see Section 5).

Due to the relatively poor quality of the right ascension least-squares fit, for the proper motion only case, we also performed a bootstrap resampling method to estimate solutions and errors more accurately. The bootstrap method resampled the data with replacement 10^4 times. We did not group the data by date, which may permit some small amount of correlated error to propagate into our solutions, i.e., as the result of same-day tropospheric corrections. In practice, we found negligible difference in the solutions (i.e., $\delta\mu_\alpha = 0.015 \text{ mas yr}^{-1}$) if we averaged the data by date before including it in the bootstrap algorithm. We adopt the bootstrap result, which is consistent with the least-squares fit but with larger errors, as our best result.

3.2. The Proper Motion and Acceleration of PSR J1745-2900

We consider initially the astrometric fits to proper motion alone. The acceleration constraints are weak and the proper-motion only fits provide the highest accuracy. The best-fit proper motion is $\mu_\alpha = 2.44 \pm 0.33 \text{ mas yr}^{-1}$ and $\mu_\delta = 5.89 \pm 0.11 \text{ mas yr}^{-1}$ (67% confidence limits). The empirical probability distribution of μ_δ is strongly peaked and resembles a Gaussian (Figure 2). The probability distribution of μ_α , on the other hand, is asymmetric with a longer tail to smaller values. The 95% confidence intervals for the best-fit parameters are $1.6 < \mu_\alpha < 3.0 \text{ mas yr}^{-1}$ and $5.7 < \mu_\delta < 6.1 \text{ mas yr}^{-1}$.

The best-fit proper motion is the opposite sign and within 25% of the magnitude of the proper motion of Sgr A* relative to the ICRF (caused by Galactic rotation). This produces the result that the pulsar is nearly at rest relative to the ICRF. Nevertheless, it is the motion of the pulsar relative to Sgr A*, which is relevant for understanding its origin and future. The transverse velocity for the pulsar relative to Sgr A* is $v = 236 \pm 11 \text{ km s}^{-1}$ in position angle 22 ± 2 deg East-of-North. From our fit, the positional offset of PSR J1745-2900 from Sgr A* at MJD 56406 (when it was first detected) was 2392 mas, corresponding to a distance of 0.097 pc. The observed separation of the pulsar is consistent with lower precision X-ray estimates (Rea et al. 2013).

The proper motion of the pulsar is similar to the motion of stars near Sgr A* studied through NIR adaptive optics (Figure 3; Yelda et al. 2014). The stars S2-4 and S2-6 are within 500 mas of PSR J1745-2900 and have proper motions of $(7.9, 3.1) \text{ mas yr}^{-1}$ and $(7.9, 2.3) \text{ mas yr}^{-1}$, respectively. The magnitude of the velocity vector is similar to that of these nearby Galactic Center stars, however, the vector orientation differs by ~ 45 deg from that of the nearest stars. This variation in the orientation is comparable to the variations among the stars. Thus, the motion of the pulsar appears to be consistent with clockwise (CW) rotation around Sgr A*. In the next section, we explore the probability of an origin in the CW stellar disk through Monte Carlo simulations and conclude that an origin in that disk is likely, although we cannot rule out an origin from the isotropic distribution of stars.

Our fits are consistent with no acceleration with 3σ upper limits of 3 mas yr^{-2} and 1.5 mas yr^{-2} in each coordinate, respectively. This does not provide a strong constraint because the maximal acceleration that can be obtained at this

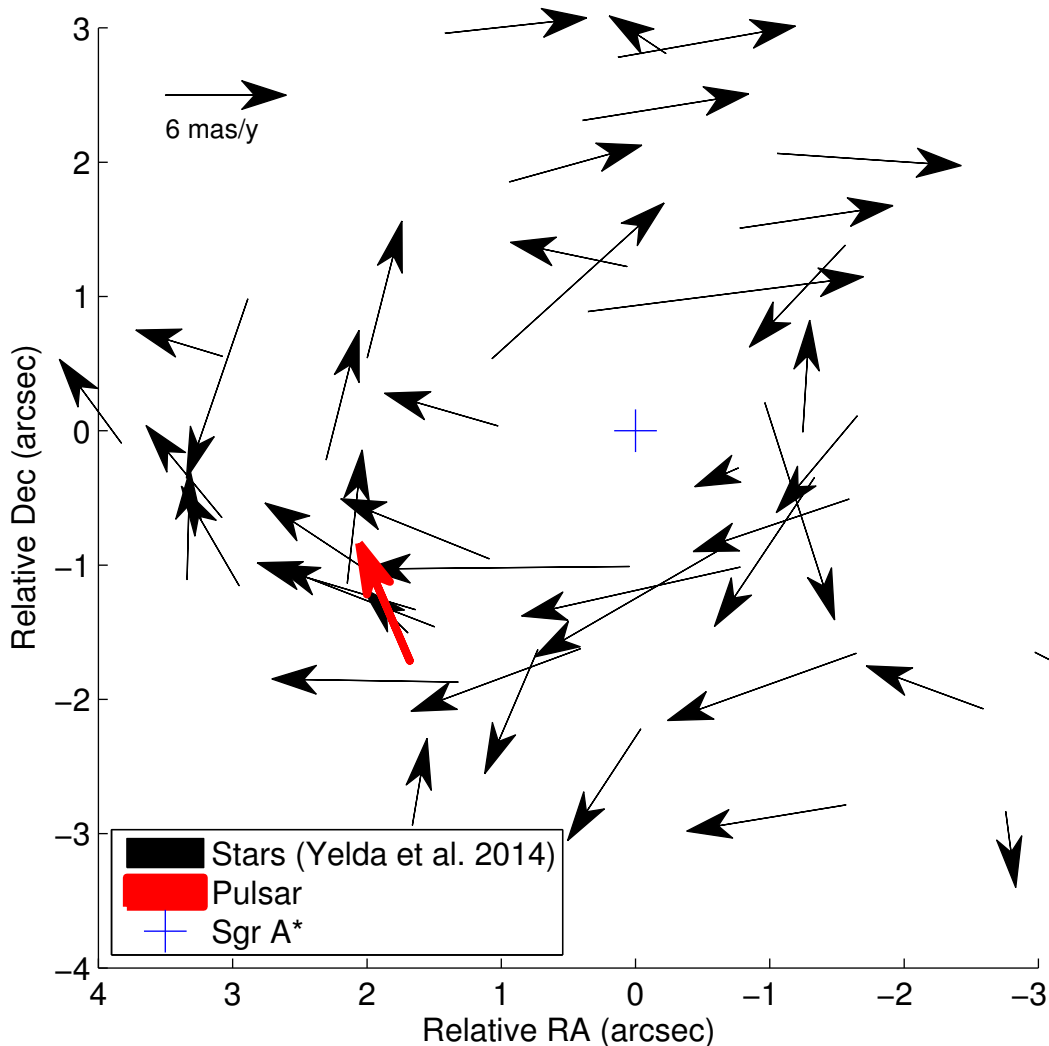


FIG. 3.— Proper motion of the pulsar along with stars from Yelda et al. (2014).

separation from Sgr A* is 0.04 mas yr^{-2} . The magnitude of the acceleration is dependent on the distance z along the line of the sight of the pulsar from Sgr A*. If the pulsar remains bright at high frequencies for $\sim 3 - 10 \text{ yr}$, future astrometric observations will have the sensitivity to detect the acceleration and, therefore, determine z . Constraints on acceleration will grow rapidly with increasing observing time.

In the absence of an acceleration, we cannot determine conclusively whether the pulsar is bound to Sgr A*. We can set limits on the velocity along the line of sight, v_z , as a function of the line of sight distance from the pulsar to Sgr A*, z , for which the pulsar is bound using the constraint that $E = T + U < 0$ (Figure 4). For $|z| < 0.1(1.0) \text{ pc}$, velocities up to $550 (170) \text{ km s}^{-1}$ are bound to Sgr A*. Faucher-Giguère & Kaspi (2006) estimate the mean natal three-dimensional velocity for pulsars at 380 km s^{-1} , corresponding to a single coordinate mean of 220 km s^{-1} . Therefore, to $|z| \lesssim 1.0 \text{ pc}$, the pulsar is likely to be bound. For $z = 0$ and $v_z = 0$, the orbital period is $\sim 700 \text{ y}$, perigee is $\sim 0.01 \text{ pc}$ and apogee is $\sim 0.1 \text{ pc}$. For higher velocities and values of z , the orbital period increases.

Two other pieces of evidence support a hypothesis that the pulsar is bound to Sgr A*. One, the chance of random superposition of an unbound object within $3''$ of Sgr A* in the $1400''$ -square Swift field of view is $\sim 10^{-5}$. Two, the relatively high transverse proper motion gives a short window $\sim 400 \text{ yr}$ in which the pulsar will be within 0.1 pc of Sgr A*. This timescale is shorter than the likely lifetime of the pulsar $\sim 10^3 - 10^4 \text{ yr}$. Thus, the observed position and velocity point to an object that is likely bound to Sgr A*.

We also set an upper limit to the parallax with a fit to the ICRF position. We find $\pi < 0.6 \text{ mas}$ at 95% confidence. The limit is poor due to the relatively limited temporal coverage and due to the systematic errors in the right ascension position. Future observations will significantly improve this limit.

3.3. Monte Carlo Simulations of the Pulsar Origin

The observed proper motion of PSR J1745-2900 is CW, consistent with the young disk of massive stars orbiting Sgr A* (Paumard et al. 2006; Lu et al. 2009; Yelda et al. 2014), however, the angle of its orbit is offset by $\approx 45 \text{ deg}$. We assess if a natal kick can move a pulsar onto this orbit using a suite of Monte Carlo simulations of potential orbits of

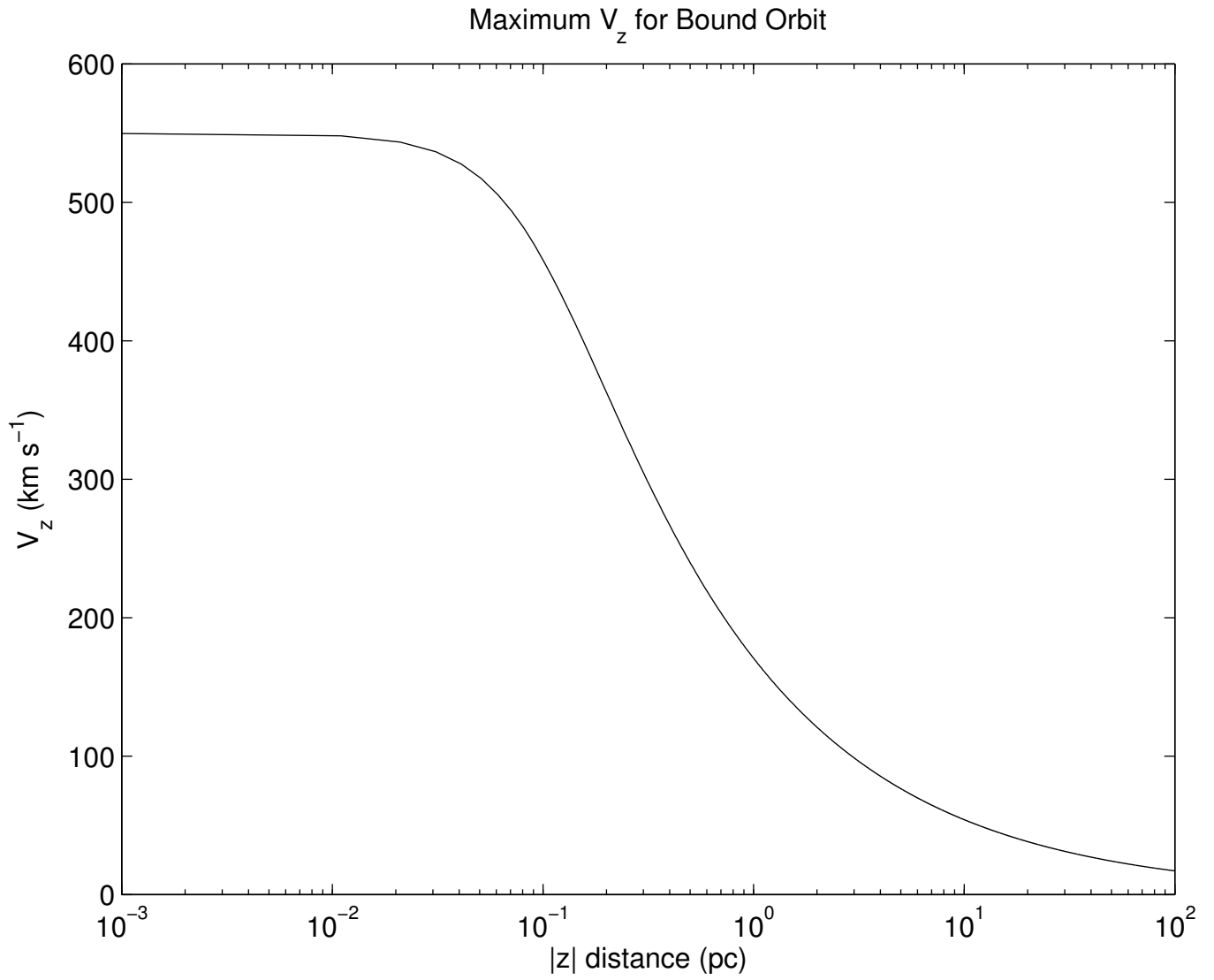


FIG. 4.— Maximum v_z as a function of $|z|$ in order for the pulsar to be bound to Sgr A*.

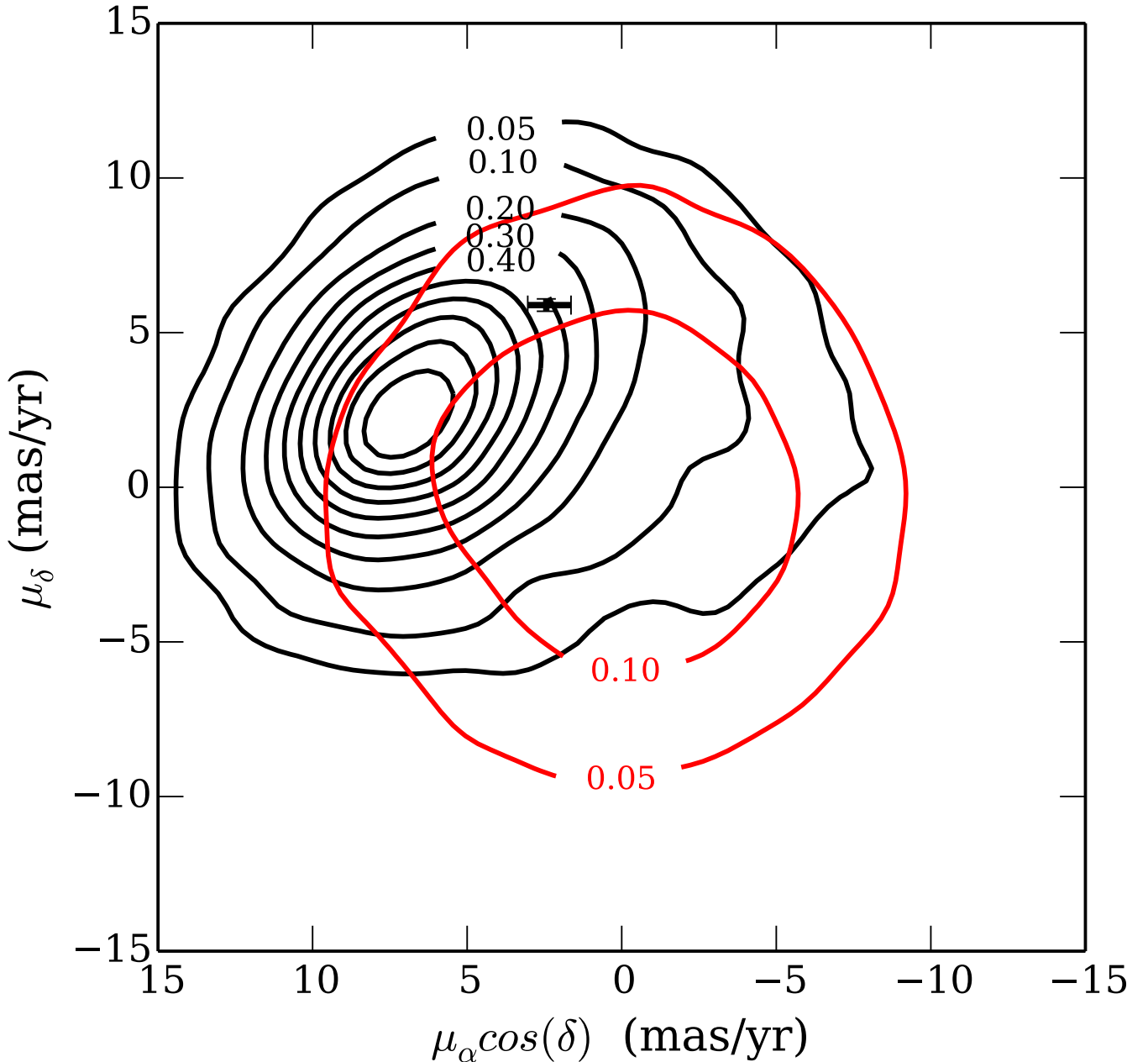


FIG. 5.— The proper motion distribution of pulsars kicked from the disk (*black lines*) and kicked from an isotropic distribution (*red lines*). Each line shows a contour of the two-dimensional probability density of proper motions for stars that are near the position of PSR J1745-2900. Nearly all the stars that originate in the disk remain on clockwise orbits around Sgr A*. The pulsar’s natal kick causes the distribution to be much broader than the observed disk of massive stars. The probability density distribution of stars that originate in the isotropic distribution is broad, and so an isotropic origin can not be excluded. The observed proper motion of PSR J1745-2900 and our 95% confidence intervals are shown with the black symbol and error bars.

pulsars in the Galactic Center assuming it originated in the stellar disk. We compare these results to Monte Carlo simulations of an alternative model of the pulsar origin, where the pulsars are kicked from an isotropic distribution of stars with a thermal distribution of eccentricities.

For the stars originating in the disk, we initially generate orbits consistent with the best fit parameters of the observed CW disk ($\Omega \approx 96 \pm 3$ deg, $i \approx 130 \pm 8$ deg, $e \approx 0.27 \pm .07$; Yelda et al. 2014). We then kick each star from its orbit by selecting a random velocity from the double-exponential distribution of Faucher-Giguère & Kaspi (2006), which has a median kick velocity of $\approx 380 \text{ km s}^{-1}$. Other distributions of pulsar kick velocities have been created with similar broad properties (e.g., Arzoumanian et al. 2002). Although this distribution was derived to fit the overall pulsar (not magnetar) population of the Milky Way, it is consistent with the observed distances of magnetars that lie near massive

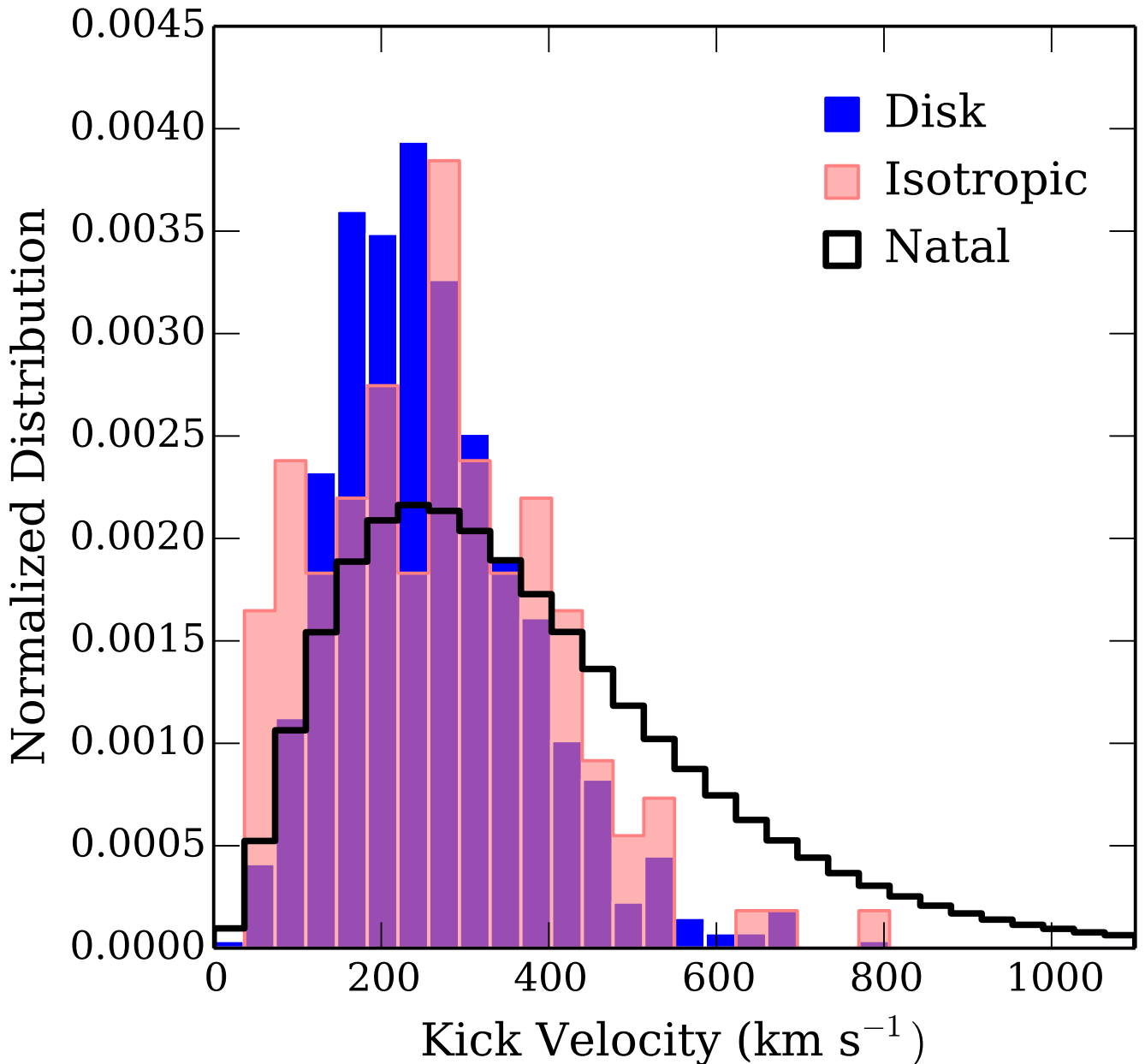


FIG. 6.— Kick velocity distribution. The natal kick velocity distribution assumed in this work is shown in black. The solid blue histogram shows the kick velocity distribution of pulsars that originated in the disk and have a similar position and proper motion to PSR J1745-2900; the same distribution for stars originating in the isotropic distribution is shown in red. For the pulsar to have originated in the disk or isotropic cloud it would require a kick of $100 - 500 \text{ km s}^{-1}$.

star forming regions and the two measured magnetar transverse velocities (Helfand et al. 2007; Deller et al. 2012). We can compare these results with stars selected from an isotropic distribution of orbits with a thermal eccentricity distribution and three-dimensional density profile $n \propto r^{-2}$ consistent with the stars not located in the disk (Paumard et al. 2006; Lu et al. 2013; Yelda et al. 2014). In both models, $\sim 10^7$ orbits are each integrated for a uniform random duration up to 10^4 yr. The longest integration time is comparable to the inferred spin-down age of PSR J1745-2900, and approximately ten orbital periods at 0.1 pc from Sgr A*; it is also slightly less than the Newtonian precession timescale at that distance (Kocsis & Tremaine 2011). As the Newtonian precession only acts in the plane of the orbit (i.e. keeps the inclination fixed), it has little impact on the currently observable properties of the magnetar, so longer integration times should not be necessary. Shorter integration times are needed to assess unbound orbits which spend little time within 0.1 pc of Sgr A*. We found no noticeable difference with the resultant distributions in using a fixed

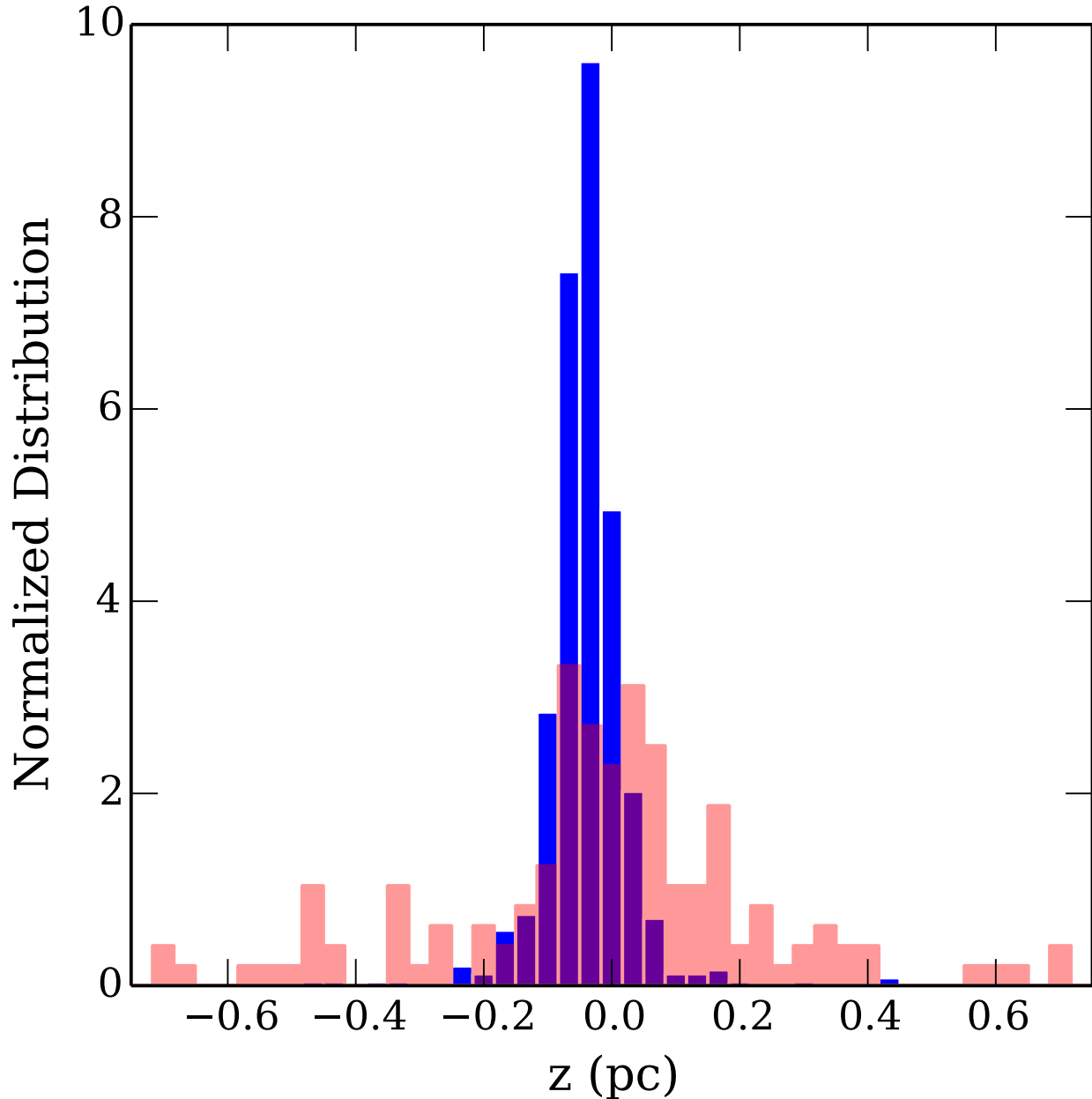


FIG. 7.— Distribution of line-of-sight distance (z) relative to Sgr A*. The solid blue histogram shows the distance for stars that were kicked out of the CW stellar disk. The red transparent histogram shows the distribution for stars that originated from an isotropic distribution. In both cases, we only show the position of pulsars with similar kinematic properties to PSR J1745-2900. Pulsars that originated in the disk are centrally concentrated with $|z| \lesssim 0.1$ pc in 88 percent of the simulations.

integration time of 10^4 or 10^5 yr. These integrations are carried out using the GALPY¹² code with a static potential that replicates the Milky Way rotation curve from the Galactic Center through the halo.

In Figure 5, we compare the observed proper motion of PSR J1745-2900 with the Monte Carlo simulations by selecting only pulsars within $1''$ of the position of PSR J1745-2900. Stars that are kicked out of the stellar disk tend to remain on CW orbits. The observed proper motion of PSR J1745-2900 is completely consistent with this distribution. The proper motion distribution of the isotropic origin, on the other hand, is rather broad, which prevents us from excluding it as the origin at a robust level. Assuming the disk fraction of stars is 50%, we find that 83% of the pulsars with kinematic properties similar to PSR J1745-2900 were born in the CW disk. However, Yelda et al. (2014) has recently revised the estimated disk fraction down to 25%. Using this lower disk fraction as our prior, lowers the

¹² <https://github.com/jobovy/galpy>

likelihood of originating from the disk to $\approx 62\%$.

Our simulations support the hypothesis that stars originating in the disk and isotropic distribution are likely to remain bound to Sgr A*. For stars originating in the disk, with the ordinary pulsar kick distribution, none of ~ 720 stars with kinematic properties similar to the magnetar were unbound to Sgr A* and central pc of stars. For stars originating from the isotropic distribution, there was 1 star out of 149 with similar kinematic properties that was unbound to the central parsec. It received a kick of 675 km s^{-1} , and was 172 years old.

Unlike in isolated massive star clusters, only very large natal kicks are sufficient to unbind a pulsar from Sgr A*. In Figure 6, we show the natal kick velocity distribution assumed in this work, to the distribution of kick velocities that resulted in magnetars with a position and proper motion similar to PSR J1745-2900. We find that the range of kicks allowed, without unbinding the magnetar spans a large range from $100 - 500 \text{ km s}^{-1}$. These limits are consistent with the finding for the four other magnetars with observed kick velocities ($\sim 130 - 350 \text{ km s}^{-1}$) are comparable to that of ordinary pulsars (Helfand et al. 2007; Deller et al. 2012; Tendulkar et al. 2012). Early models predicted that magnetar birth kicks could be much larger than those of normal pulsars, enabled by exotic kick mechanisms that could not operate efficiently in the formation of normal pulsars (Duncan & Thompson 1992; Thompson & Duncan 1993); our results for PSR J1745-2900 add further evidence disfavoring these predictions. On its own this one transverse velocity does not strongly constrain the natal kick velocity distribution of magnetars, but three measurements which each require unlikely viewing geometries to support a natal kick in excess of 500 km s^{-1} strongly disfavor a distribution which peaks at high velocities ($> 500 \text{ km s}^{-1}$). On its own this one kick measurement does not provide much constraint on the natal kick velocity, but three kick measurements in which the kick is either $< 500 \text{ km s}^{-1}$ or the alignment is very fortuitous is unlikely. It is difficult to give a quantitative estimate, since the width and functional form of the velocity distribution would also be free parameters, but a simple assumption like the scaling up of the Maxwellian distribution assumed for normal pulsars to give a $2\times$ higher kick (and hence a mean 3d kick velocity of 800 km s^{-1} vs 400 km s^{-1}) gives a probability of sampling 5 magnetars with transverse velocity measurements $< 300 \text{ km s}^{-1}$ of $\lesssim 0.1\%$.

In Figure 7, we show the expected distance of PSR J1745-2900 relative to Sgr A* assuming it formed in a disk or from an isotropic distribution. At PSR J1745-2900's current position, stars in the CW stellar disk are nearest us and have measured positive radial velocities. We find that if the magnetar originated in the disk, it has $|z| \lesssim 0.1 \text{ pc}$ in 88% of the simulations. If the magnetar originated from an isotropic distribution of stars we find it still has $|z| \lesssim 0.1 \text{ pc}$ and a proper motion comparable to the measured value in $\approx 49\%$ of our simulations. As noted above, future interferometric observations of PSR J1745-2900 will likely detect the acceleration of PSR J1745-2900 and determine $|z|$.

4. IMPLICATIONS FOR SGR A*

4.1. Size Fits for PSR J1745-2900 and Sgr A*

We plot the observed size of the pulsar as a function of wavelength in Figure 8. The pulsar size shows excellent agreement from 3.6 cm to 0.7 cm with the scattering model for Sgr A* in both major and minor axes. This result further supports the angular broadening interpretation of Bower et al. (2014a) that the pulsar and Sgr A* share the same scattering medium along the line of sight. The similarity over all wavelengths is important because it demonstrates that the mean scattering properties of either source will not change for a time scale $\tau \gtrsim R/v \sim 1000 \text{ yr}$, where $R \sim 0.1 \text{ pc}$ is the separation between the pulsar and Sgr A* and $v \sim 100 \text{ km s}^{-1}$ is the velocity of the scattering screen across the line of sight. This timescale is much larger than the refractive timescale $\tau_R \sim 0.05 \text{ yr}$ at 7mm, indicating that the scattering medium appears to be smooth over large scales.

We also find new constraints on the size of Sgr A* from closure amplitude analysis of visibilities. Closure amplitude analysis provides the most accurate method for determining the size of Sgr A* (Bower et al. 2014b). We provide new results for the size at 3.5 and 2.0 cm that are a substantial improvement on sizes previously measured (Bower et al. 2004). Improvements are due to the greater bandwidth and, therefore, improved sensitivity of VLBA observations and the inclusion of the VLA which provides shorter baselines. At both wavelengths, the new measured major axis sizes are more precise and differ by less than 2σ with the earlier measured sizes. Any differences could be due to changes in the intrinsic size or in the refractive properties of the medium. Including the new 3.5 cm major axis size with the earlier 6 cm VLBA size and L-band VLA sizes from Bower et al. (2006), we estimate the major axis scattering normalization $b_{maj,scatt} = 1.32 \pm 0.02 \text{ mas cm}^{-1}$. This is consistent within the errors with the previous estimate of $b_{maj,scatt}$. The new minor axis sizes at 3.5 and 2.0 cm are a significant improvement over previous values. We combine these measurements with the previous 6 cm VLBA size but not the L-band VLA minor axis sizes, which were corrupted by the presence of a radio transient, and find a new estimate of the minor axis scattering normalization, $b_{min,scatt} = 0.67 \pm 0.02 \text{ mas cm}^{-1}$. The error is a factor of two smaller than previous estimates. We also estimate the mean position angle from the 2 to 6 cm data to be $81.8 \pm 0.2 \text{ deg}$. These new estimates are more precise but within the errors of previous estimates and so do not affect significantly conclusions on the intrinsic size of Sgr A* (e.g., Falcke et al. 2009; Bower et al. 2014b).

4.2. Core Shift in Sgr A*

The core shift arises in jet sources because the optical depth changes as a function of wavelength (Blandford & Konigl 1979; Falcke & Biermann 1995). At shorter wavelengths, jets appear more compact and the $\tau = 1$ surface is closer to the origin of the jet and, therefore, the black hole. We phase-reference the pulsed emission from PSR J1745-2900 to Sgr A* in this experiment. The pulsed emission must be intrinsically point-like since it originates within the pulsar magnetosphere, which has an angular size smaller than $1 \mu\text{as}$. Thus, any wavelength-dependence in the position of the

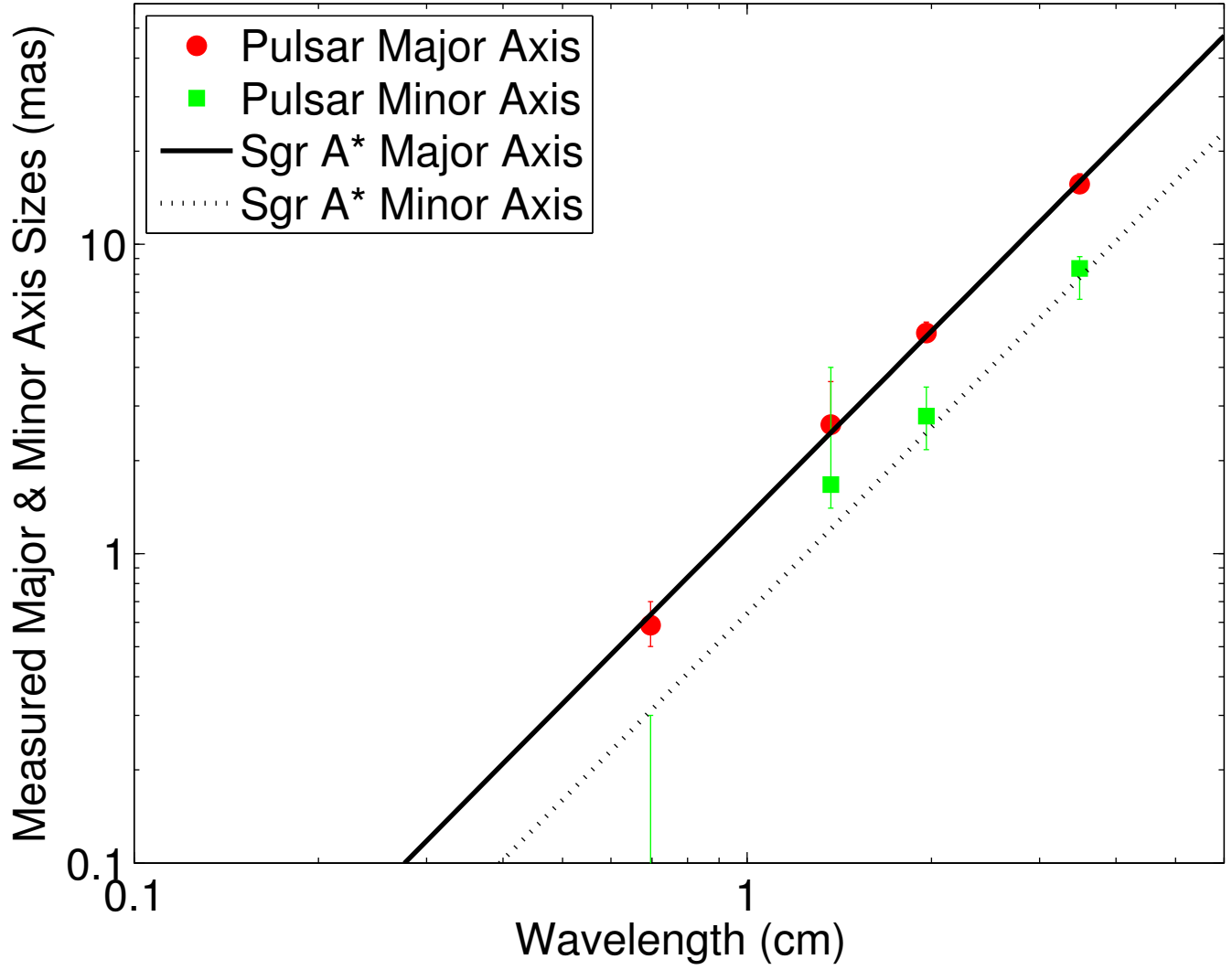


FIG. 8.— Pulsar size as a function of wavelength for major and minor axes. Data are plotted against the fitted major and minor axis size of Sgr A*, which scales as λ^2 .

pulsar must originate from wavelength-dependent structures in Sgr A*. The discovery of refractive substructure by Gwinn et al. (2014), however, does suggest that differential image wander could also affect this relative measurement. Many accretion models for Sgr A* suggest that the accretion flow is likely to be spherically symmetric and, therefore, produce zero core shift. Our data provides a powerful opportunity to probe the structure of Sgr A* at wavelengths where the source image is strongly dominated by interstellar scattering. We define the core shift Φ in Equation 2 for right ascension and declination as a wavelength scaling to the position.

As Table 4 demonstrates, our least-squares fit does not find a significant detection of a constant core shift. The 3σ upper limit is $\sim 0.3 \text{ mas cm}^{-1}$ in right ascension and $\sim 0.2 \text{ mas cm}^{-1}$ in declination. The fit to all data is heavily weighted by the high SNR detections at wavelengths of 1.3 and 0.7 cm. Giving equal weight to all epochs in the fit also does not lead to a statistically significant detection. We also consider the possibility that the core shift may be time variable. Sgr A* is known to have time variable flux density at all wavelengths, including the longer wavelengths examined here (Herrnstein et al. 2004; Macquart & Bower 2006). In five epochs (MJD 56658, 56710, 56750, 56772, and 56899), we obtain simultaneous observations at two wavelengths from which we can estimate a core shift (Figure 9). For three of these epochs, the two bands are Ku and X; in the fourth and fifth epoch, the bands are K and Q. In only one epochs (MJD 56772, Ku and X band) do we see a $> 3\sigma$ core shift with an amplitude $\sim -0.4 \text{ mas cm}^{-1}$; for epoch MJD 56899, K and Q band, the significance is $\sim 2.8\sigma$ with a value of 0.7 mas cm^{-1} . Errors in Φ are determined using the formal statistical errors on the measured positions rather than errors scaled to achieve $\chi^2_\nu = 1$, because we are testing the question of whether apparent systematics offsets may be due to the core shift. Given the large scatter in the core shift measurements and systematic error in the right ascension positions, we conclude that we have produced an upper bound on the amplitude of the core shift. Higher sensitivity measurements with three or more simultaneous frequencies are necessary to convincingly demonstrate the presence (or absence) of a core shift. Multi-frequency measurements could also test against refractive effects due to large-scale inhomogeneities in the scattering screen leading the positions for the two sources to wander independently.

The sign and angle of the coreshift is indicative of the direction of a jet. If our single epoch detection of the core shift is accurate, this indicates a jet that extends primarily to the Southwest in position angle 245 deg East of North. Bower et al. (2014b) found an extension of the source in position angle ~ 95 deg, which is not statistically consistent with the direction of the core shift. There is also some suggestion in the data of an alignment of the individual epochs along the 245 deg axis, which could be consistent with a time-variable bipolar outflow.

We compare the measurements with the core shift predictions presented in Mościbrodzka et al. (2014). The theoretical models are based on the general relativistic magnetohydrodynamics simulations of an accreting black hole in which jets are naturally produced by magnetic processes. These simulations combined with the ray-tracing radiative transfer models can predict the synthetic images of the jet-disk-black hole triad at various wavelengths (Mościbrodzka & Falcke 2013; Mościbrodzka et al. 2014). To compute the theoretical core shifts, the time-averaged images of the jet models are convolved with the scattering screen Gaussian for various position angles (PA) of the jet on the sky. Then, the theoretical core shift is $\Phi_{theory}(PA) = (\phi_1(PA) - \phi_2(PA))/(\lambda_1 - \lambda_2)$, where $\phi_{1,2}$ are the centroids of the scattering-broadened images at $\lambda_{1,2}=0.7$ and 1.3 cm, respectively. The theoretical core shifts for a jet inclined at $i = 60$ deg and various PA are shown in Figure 9. We have chosen to show this model because its broadband synthetic spectrum and image size at mm-wavelength are consistent with all observations of Sgr A*. Other self-consistent models may show different profiles. We find that the model time-averaged core shifts are of the same order of magnitude ($\sim 0.2 \text{ mas cm}^{-1}$) as those measured only during individual epochs of our observations. One can further test the time-dependent GRMHD models of jets by studying the core shift as a function of time. A variable core shift puts strong constraints on the jet particle heating, its speed, and inclination angle but this requires more detailed investigation.

We also consider a simple order of magnitude estimate of the amplitude of the core shift based on measured time lags in variability for Sgr A*. Yusef-Zadeh et al. (2006) observed delays of $\tau \sim 30$ minutes between variability at 1.3 and 0.7 cm. If these delays represent the size of the photosphere at different wavelengths and the underlying structure is a jet with velocity v_j and inclination angle of 90 deg, then the apparent core shift is $\Phi \sim v_j \tau / D_{GC} / \Delta \lambda$ (Falcke et al. 2009), where $D_{GC} = 8.3$ kpc is the distance to the Galactic Center. We find $\Phi \approx 0.7(v_j/c) \text{ mas cm}^{-1}$, which is a comparable order of magnitude to the detailed model estimates and our measured values.

5. DISCUSSION AND CONCLUSIONS

We have shown that the magnetar most likely originated within the CW stellar disk orbiting Sgr A*, or, with less likelihood, the isotopic stellar population at a radius $\lesssim 0.4$ pc. This statement rests on the assumption that the natal kick velocity distribution for magnetars is similar to that of ordinary pulsars, which this result appears to support. Both populations are a part of the Galactic Center cluster, which consists of numerous O and WR stars with a characteristic age of ~ 4 Myr and a total mass $> 10^4 M_\odot$; the most massive existing stars have initial masses up to $\sim 60 M_\odot$ (Paumard et al. 2006; Lu et al. 2013). This supports the identification of magnetars as the remnants of supernova explosions of high mass stars.

Single stars appear to primarily create black holes for initial masses greater than $25 M_\odot$, but binarity appears to create a pathway for greater mass loss leading to neutron star and possibly magnetar formation (Fryer et al. 2002; Belczynski & Taam 2008). This was recently demonstrated by the discovery of a potential binary companion to the progenitor of the magnetar J1647-45 in Westerlund 1 (Wd 1; Munro et al. 2006; An et al. 2013; Clark et al. 2014). Massive binary stars in the central few arcseconds of the Galactic Center cluster have been detected in three systems: IRS 16SW, IRS 16NE, and E-60 (also known as S4-258; Pfuhl et al. 2014). E-60 and IRS 16SW are contact binaries,

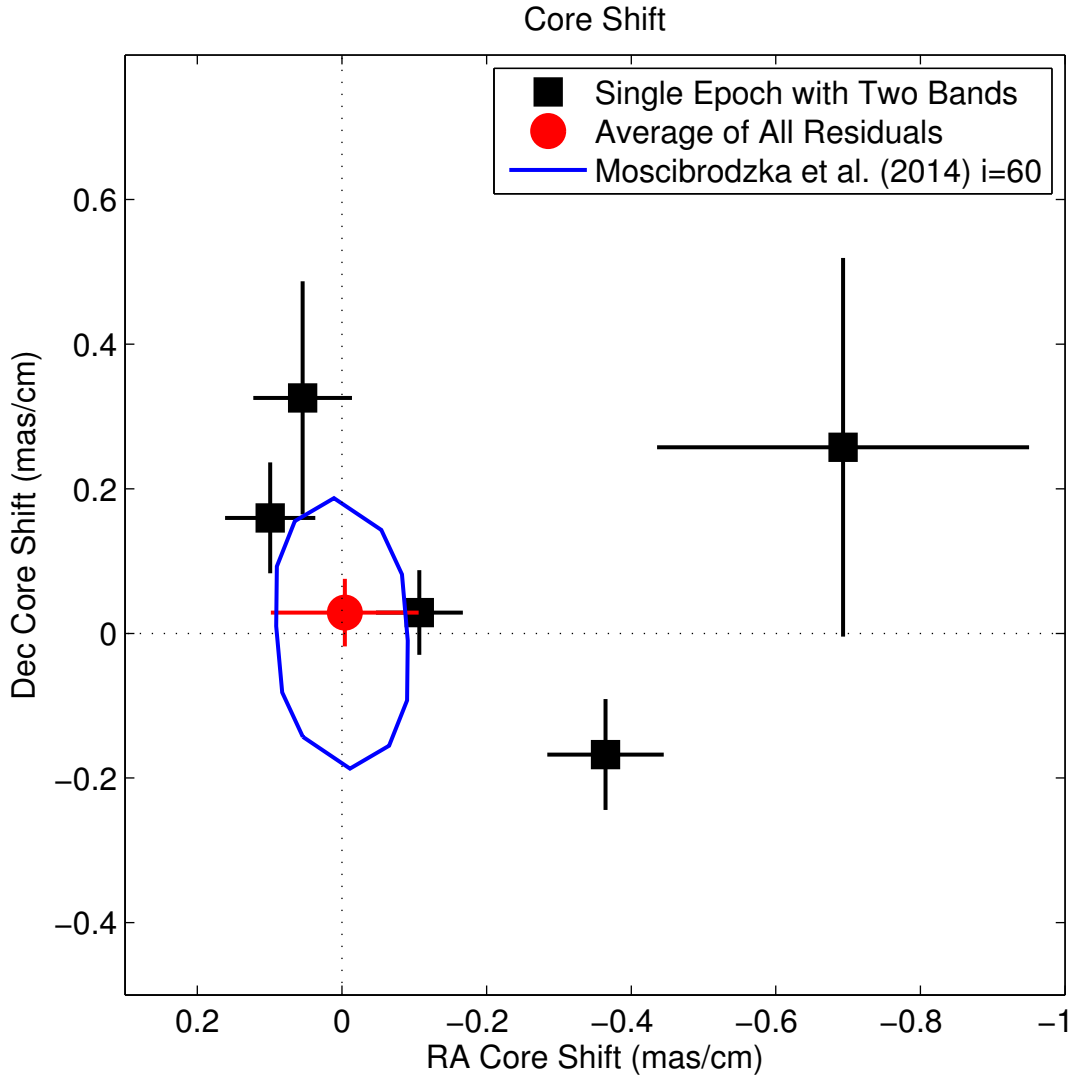


FIG. 9.— Core shift for the four individual epochs with two frequency observations (black squares) and for the average over all epochs (red circle). The blue curve shows the core shift estimated from GRMHD jet simulations with an inclination angle of 60 deg oriented towards different position angles. Models are convolved with the scattering beam and then the centroids are determined. The measured and theoretical core shifts agree in order of magnitude.

which may be necessary for the co-evolution of massive stars leading to a magnetar (Fryer et al. 2002; Clark et al. 2014). Co-evolution can lead to mass loss in the supernova progenitor, which reduces angular momentum loss in the core during the final stages of stellar evolution and, thereby, enhancing the seed magnetic field required for magnetar production. The binary fraction among massive stars in the Galactic Center cluster is estimated to be substantial and comparable to that seen in other dense clusters. None of the known binary systems, however, are given a high probability of membership in the CW stellar disk (Yelda et al. 2014); E-60 appears to be marginally bound or unbound to Sgr A*. Nevertheless, it is not unreasonable to argue that the pulsar originated in a massive binary system in the CW stellar disk. We note that one of the pulsars in the central 40 pc of the Galaxy, PSR J1746-2850II, also appears to be a young, highly magnetized neutron star with a possible origin in the Arches or Quintuplet cluster (Deneva et al. 2009). The other known pulsars are ordinary, long-period sources, whose origin could be in one of the young stellar clusters or in other regions in the Galactic Center.

The association of the pulsar with an origin in the CW stellar disk supports the basic theory behind predictions of the population of neutron stars, black holes, and pulsars in the Galactic Center. The young stars in the Galactic Center are expected to produce many compact objects as they evolve through the supernova phase. Such pulsars are expected to be produced and should have been detected through existing surveys but they are not present. Given the low overall fraction of magnetars among field pulsars ($\lesssim 10^{-2}$; Chennamangalam & Lorimer 2014), identification of the first Galactic Center pulsar as a magnetar is surprising. Note that while the X-ray outburst made quick radio discovery of PSR J1745-2900 possible, the many radio pulsar searches over the past decades would have readily found the magnetar as well as the more stably emitting ordinary pulsars. If massive stars in binary systems are common in the Galactic Center cluster and efficiently form magnetars, however, the association of PSR J1745-2900 with the local stellar cluster may resolve this anomaly. This resolution requires that we are at an early stage of high-mass star formation following a period of relative inactivity comparable to the characteristic pulsar lifetime (~ 10 Myr) in which few pulsars were formed. In this scenario, the young pulsar population of the Galactic Center resembles that of a star-forming cluster similar to Wd 1, which has no radio pulsars. As the cluster ages, lower mass stars will go through a supernova phase and produce ordinary pulsars (i.e., non-magnetars).

The star formation history of the Galactic Center cluster over the age of the Galaxy has been extensively studied (e.g., Blum et al. 2003; Pfuhl et al. 2011). Evolved giant branch stars appear to reveal a significant rise in the star formation rate over the past few hundred million years, reaching the current peak of $\sim 10^{-2} M_{\odot} \text{ yr}^{-1}$. The star formation rate 100 Myr in the past is an order of magnitude lower than the current rate. The granularity of star-formation rate determination with this method is fairly coarse, however, with characteristic widths of approximately 100 Myr. On the other hand, study of high mass stars indicates a burst of star formation no earlier than 6 Myr in the past (Lu et al. 2013), i.e., indicating variability in the star formation rate on time scales comparable to the pulsar lifetime.

Magnetar formation is poorly understood and based on a relatively small sample of objects. For instance, evidence has been presented that some ordinary pulsars may evolve into magnetars (Espinoza et al. 2011). Considering also the complex star-formation history of the Galactic Center, we cannot present a definitive account of the origin of PSR J1745-2900 and pulsars in the vicinity of Sgr A*. Nevertheless, the anomaly of the first Galactic Center pulsar appearing as a magnetar and the apparently insufficient strength of the scattering screen to obscure ordinary pulsars is plausibly resolved through a scenario in which magnetars are the earliest pulsars formed in the young Galactic Center cluster.

Millisecond pulsars (MSPs) from previous generations of star formation, on the other hand, should be present and would still have escaped detection in existing surveys. Even with the reduced temporal broadening estimate based on a greater distance to the scattering screen, detection of MSPs requires high frequency, high sensitivity observations. MSPs, therefore, provide the potential for the characterization of general relativistic effects associated with Sgr A*. Efforts are underway to search for MSPs at frequencies above 10 GHz with the VLA, GBT, and Effelsberg (Siemion et al. 2013; Eatough et al. 2013b); an SKA-sized array built with high frequency receivers or ALMA (Fish et al. 2013) may have the capability to detect MSPs if current efforts are unsuccessful.

The National Radio Astronomy Observatory is a facility of the National Science Foundation operated under cooperative agreement by Associated Universities, Inc.

REFERENCES

- An, H., Kaspi, V. M., Archibald, R., & Cumming, A. 2013, *ApJ*, 763, 82
 Arzoumanian, Z., Chernoff, D. F., & Cordes, J. M. 2002, *ApJ*, 568, 289
 Backer, D. C. & Hellings, R. W. 1986, *ARA&A*, 24, 537
 Belczynski, K. & Taam, R. E. 2008, *ApJ*, 685, 400
 Bietenholz, M. F., Bartel, N., & Rupen, M. P. 2004, *ApJ*, 615, 173
 Blandford, R. D. & Konigl, A. 1979, *ApJ*, 232, 34
 Blum, R. D., Ramírez, S. V., Sellgren, K., & Olsen, K. 2003, *ApJ*, 597, 323
 Bower, G. C., Deller, A., Demorest, P., Brunthaler, A., Eatough, R., Falcke, H., Kramer, M., Lee, K. J., & Spitler, L. 2014a, *ApJ*, 780, L2
 Bower, G. C., Falcke, H., Herrnstein, R. M., Zhao, J., Goss, W. M., & Backer, D. C. 2004, *Science*, 304, 704
 Bower, G. C., Goss, W. M., Falcke, H., Backer, D. C., & Lithwick, Y. 2006, *ApJ*, 648, L127
 Bower, G. C., Markoff, S., Brunthaler, A., Law, C., Falcke, H., Maitra, D., Clavel, M., Goldwurm, A., Morris, M. R., Witzel, G., Meyer, L., & Ghez, A. M. 2014b, *ApJ*, 790, 1

- Bower, G. C., Roberts, D. A., Yusef-Zadeh, F., Backer, D. C., Cotton, W. D., Goss, W. M., Lang, C. C., & Lithwick, Y. 2005, *ApJ*, 633, 218
- Bramante, J. & Linden, T. 2014, *ArXiv e-prints*, 1405.1031
- Broderick, A. E. & Loeb, A. 2006, *ApJ*, 636, L109
- Chennamangalam, J. & Lorimer, D. R. 2014, *MNRAS*, 440, L86
- Clark, J. S., Ritchie, B. W., Najarro, F., Langer, N., & Negueruela, I. 2014, *A&A*, 565, A90
- Cordes, J. M., Kramer, M., Lazio, T. J. W., Stappers, B. W., Backer, D. C., & Johnston, S. 2004, *New A Rev.*, 48, 1413
- Deller, A. T., Camilo, F., Reynolds, J. E., & Halpern, J. P. 2012, *ApJ*, 748, L1
- Deneva, J. S., Cordes, J. M., & Lazio, T. J. W. 2009, *ApJ*, 702, L177
- Dexter, J. & O'Leary, R. M. 2014, *ApJ*, 783, L7
- Doeleman, S. S., Weintroub, J., Rogers, A. E. E., Plambeck, R., Freund, R., Tilanus, R. P. J., Friberg, P., Ziurys, L. M., Moran, J. M., Corey, B., Young, K. H., Smythe, D. L., Titus, M., Marrone, D. P., Cappallo, R. J., Bock, D., Bower, G. C., Chamberlin, R., Davis, G. R., Krichbaum, T. P., Lamb, J., Maness, H., Niell, A. E., Roy, A., Strittmatter, P., Werthimer, D., Whitney, A. R., & Woody, D. 2008, *Nature*, 455, 78
- Duncan, R. C. & Thompson, C. 1992, *ApJ*, 392, L9
- Eatough, R. P., Falcke, H., Karuppusamy, R., Lee, K. J., Champion, D. J., Keane, E. F., Desvignes, G., Schnitzeler, D. H. F. M., Spitler, L. G., Kramer, M., Klein, B., Bassa, C., Bower, G. C., Brunthaler, A., Cognard, I., Deller, A. T., Demorest, P. B., Freire, P. C. C., Kraus, A., Lyne, A. G., Noutsos, A., Stappers, B., & Wex, N. 2013a, *Nature*, 501, 391
- Eatough, R. P., Kramer, M., Klein, B., Karuppusamy, R., Champion, D. J., Freire, P. C. C., Wex, N., & Liu, K. 2013b, in *IAU Symposium*, Vol. 291, *IAU Symposium*, 382-384
- Espinoza, C. M., Lyne, A. G., Kramer, M., Manchester, R. N., & Kaspi, V. M. 2011, *ApJ*, 741, L13
- Falcke, H. 1999, in *Astronomical Society of the Pacific Conference Series*, Vol. 186, *The Central Parsecs of the Galaxy*, ed. H. Falcke, A. Cotera, W. J. Duschl, F. Melia, & M. J. Rieke, 148
- Falcke, H. & Biermann, P. L. 1995, *A&A*, 293, 665
- Falcke, H., Markoff, S., & Bower, G. C. 2009, *A&A*, 496, 77
- Faucher-Giguère, C.-A. & Kaspi, V. M. 2006, *ApJ*, 643, 332
- Fish, V., Alef, W., Anderson, J., Asada, K., Baudry, A., Broderick, A., Carilli, C., Colomer, F., Conway, J., Dexter, J., Doeleman, S., Eatough, R., Falcke, H., Frey, S., Gabányi, K., Gálvan-Madrid, R., Gammie, C., Giroletti, M., Goddi, C., Gómez, J. L., Hada, K., Hecht, M., Honma, M., Humphreys, E., Impellizzeri, V., Johannsen, T., Jorstad, S., Kino, M., Körding, E., Kramer, M., Krichbaum, T., Kudryavtseva, N., Laing, R., Lazio, J., Loeb, A., Lu, R.-S., Maccarone, T., Marscher, A., Mart'ı-Vidal, I., Martins, C., Matthews, L., Menten, K., Miller, J., Miller-Jones, J., Mirabel, F., Muller, S., Nagai, H., Nagar, N., Nakamura, M., Paragi, Z., Pradel, N., Psaltis, D., Ransom, S., Rodr'ıguez, L., Rottmann, H., Rushton, A., Shen, Z.-Q., Smith, D., Stappers, B., Takahashi, R., Tarchi, A., Tilanus, R., Verbiest, J., Vlemmings, W., Walker, R. C., Wardle, J., Wiik, K., Zackrisson, E., & Zensus, J. A. 2013, *ArXiv e-prints*
- Fish, V. L., Doeleman, S. S., Beaudoin, C., Blundell, R., Bolin, D. E., Bower, G. C., Chamberlin, R., Freund, R., Friberg, P., Gurwell, M. A., Honma, M., Inoue, M., Krichbaum, T. P., Lamb, J., Marrone, D. P., Moran, J. M., Oyama, T., Plambeck, R., Primiani, R., Rogers, A. E. E., Smythe, D. L., SooHoo, J., Strittmatter, P., Tilanus, R. P. J., Titus, M., Weintroub, J., Wright, M., Woody, D., Young, K. H., & Ziurys, L. M. 2011, *ApJ*, 727, L36
- Frail, D. A., Diamond, P. J., Cordes, J. M., & van Langevelde, H. J. 1994, *ApJ*, 427, L43
- Freitag, M., Amaro-Seoane, P., & Kalogera, V. 2006, *ApJ*, 649, 91
- Fryer, C. L., Heger, A., Langer, N., & Wellstein, S. 2002, *ApJ*, 578, 335
- Goodman, J. & Narayan, R. 1989, *MNRAS*, 238, 995
- Greisen, E. W. 2003, in *Astrophysics and Space Science Library*, Vol. 285, *Astrophysics and Space Science Library*, ed. A. Heck, 109
- Gwinn, C. R., Kovalev, Y. Y., Johnson, M. D., & Soglasnov, V. A. 2014, *ArXiv e-prints*
- Gwinn, C. R., Moran, J. M., Reid, M. J., & Schneps, M. H. 1988, *ApJ*, 330, 817
- Hada, K., Doi, A., Kino, M., Nagai, H., Hagiwara, Y., & Kawaguchi, N. 2011, *Nature*, 477, 185
- Helfand, D. J., Chatterjee, S., Brisken, W. F., Camilo, F., Reynolds, J., van Kerkwijk, M. H., Halpern, J. P., & Ransom, S. M. 2007, *ApJ*, 662, 1198
- Herrnstein, R. M., Zhao, J.-H., Bower, G. C., & Goss, W. M. 2004, *AJ*, 127, 3399
- Johnston, S., Kramer, M., Lorimer, D. R., Lyne, A. G., McLaughlin, M., Klein, B., & Manchester, R. N. 2006, *MNRAS*, 373, L6
- Kaspi, V. M., Archibald, R. F., Bhalerao, V., Dufour, F., Gotthelf, E. V., An, H., Bachetti, M., Beloborodov, A. M., Boggs, S. E., Christensen, F. E., Craig, W. W., Grefenstette, B. W., Hailey, C. J., Harrison, F. A., Kennea, J. A., Kouveliotou, C., Madsen, K. K., Mori, K., Markwardt, C. B., Stern, D., Vogel, J. K., & Zhang, W. W. 2014, *ApJ*, 786, 84
- Kennea, J. A., Burrows, D. N., Kouveliotou, C., Palmer, D. M., Göğüş, E., Kaneko, Y., Evans, P. A., Degenaar, N., Reynolds, M. T., Miller, J. M., Wijnands, R., Mori, K., & Gehrels, N. 2013, *ApJ*, 770, L24
- Kocsis, B. & Tremaine, S. 2011, *MNRAS*, 412, 187
- Kramer, M., Klein, B., Lorimer, D., Müller, P., Jessner, A., & Wielebinski, R. 2000, in *Astronomical Society of the Pacific Conference Series*, Vol. 202, *IAU Colloq. 177: Pulsar Astronomy - 2000 and Beyond*, ed. M. Kramer, N. Wex, & R. Wielebinski, 37
- Liu, K., Wex, N., Kramer, M., Cordes, J. M., & Lazio, T. J. W. 2012, *ApJ*, 747, 1
- Lo, K. Y., Shen, Z. Q., Zhao, J. H., & Ho, P. T. P. 1998, *ApJ*, 508, L61
- Lu, J. R., Do, T., Ghez, A. M., Morris, M. R., Yelda, S., & Matthews, K. 2013, *ApJ*, 764, 155
- Lu, J. R., Ghez, A. M., Hornstein, S. D., Morris, M. R., Becklin, E. E., & Matthews, K. 2009, *ApJ*, 690, 1463
- Macquart, J.-P. & Bower, G. C. 2006, *ApJ*, 641, 302
- Macquart, J.-P., Kanekar, N., Frail, D. A., & Ransom, S. M. 2010, *ApJ*, 715, 939
- Mori, K., Gotthelf, E. V., Zhang, S., An, H., Baganoff, F. K., Barrière, N. M., Beloborodov, A. M., Boggs, S. E., Christensen, F. E., Craig, W. W., Dufour, J., Grefenstette, B. W., Hailey, C. J., Harrison, F. A., Hong, J., Kaspi, V. M., Kennea, J. A., Madsen, K. K., Markwardt, C. B., Nynka, M., Stern, D., Tomsick, J. A., & Zhang, W. W. 2013, *ApJ*, 770, L23
- Mościbrodzka, M. & Falcke, H. 2013, *A&A*, 559, L3
- Mościbrodzka, M., Falcke, H., Shiohara, H., & Gammie, C. F. 2014, *A&A*, submitted
- Muno, M. P., Baganoff, F. K., Brandt, W. N., Morris, M. R., & Starck, J.-L. 2008, *ApJ*, 673, 251
- Muno, M. P., Bauer, F. E., Baganoff, F. K., Bandyopadhyay, R. M., Bower, G. C., Brandt, W. N., Broos, P. S., Cotera, A., Eikenberry, S. S., Garmire, G. P., Hyman, S. D., Kassim, N. E., Lang, C. C., Lazio, T. J. W., Law, C., Mauerhan, J. C., Morris, M. R., Nagata, T., Nishiyama, S., Park, S., Ramirez, S. V., Stolovy, S. R., Wijnands, R., Wang, Q. D., Wang, Z., & Yusef-Zadeh, F. 2009, *ApJS*, 181, 110
- Muno, M. P., Clark, J. S., Crowther, P. A., Dougherty, S. M., de Grijs, R., Law, C., McMillan, S. L. W., Morris, M. R., Negueruela, I., Pooley, D., Portegies Zwart, S., & Yusef-Zadeh, F. 2006, *ApJ*, 636, L41
- Muno, M. P., Pfahl, E., Baganoff, F. K., Brandt, W. N., Ghez, A., Lu, J., & Morris, M. R. 2005, *ApJ*, 622, L113
- Narayan, R. & Goodman, J. 1989, *MNRAS*, 238, 963
- Paumard, T., Genzel, R., Martins, F., Nayakshin, S., Beloborodov, A. M., Levin, Y., Trippe, S., Eisenhauer, F., Ott, T., Gillessen, S., Abuter, R., Cuadra, J., Alexander, T., & Sternberg, A. 2006, *ApJ*, 643, 1011
- Pfahl, E. & Loeb, A. 2004, *ApJ*, 615, 253
- Pfuhl, O., Alexander, T., Gillessen, S., Martins, F., Genzel, R., Eisenhauer, F., Fritz, T. K., & Ott, T. 2014, *ApJ*, 782, 101
- Pfuhl, O., Fritz, T. K., Zilka, M., Maness, H., Eisenhauer, F., Genzel, R., Gillessen, S., Ott, T., Dodds-Eden, K., & Sternberg, A. 2011, *ApJ*, 741, 108

- Rea, N., Esposito, P., Pons, J. A., Turolla, R., Torres, D. F., Israel, G. L., Possenti, A., Burgay, M., Viganò, D., Papitto, A., Perna, R., Stella, L., Ponti, G., Baganoff, F. K., Haggard, D., Camero-Arranz, A., Zane, S., Minter, A., Mereghetti, S., Tiengo, A., Schödel, R., Feroci, M., Mignani, R., & Götz, D. 2013, *ApJ*, 775, L34
- Reid, M. J., Broderick, A. E., Loeb, A., Honma, M., & Brunthaler, A. 2008, *ApJ*, 682, 1041
- Reid, M. J. & Brunthaler, A. 2004, *ApJ*, 616, 872
- Reid, M. J. & Honma, M. 2014, *ARA&A*, 52, 339
- Shannon, R. M. & Johnston, S. 2013, *MNRAS*, 435, L29
- Shepherd, M. C. 1997, in *Astronomical Society of the Pacific Conference Series*, Vol. 125, *Astronomical Data Analysis Software and Systems VI*, ed. G. Hunt & H. Payne, 77
- Siemion, A., Bailes, M., Bower, G., Chennamangalam, J., Cordes, J., Demorest, P., Deneva, J., Desvignes, G., Ford, J., Frail, D., Jones, G., Kramer, M., Lazio, J., Lorimer, D., McLaughlin, M., Ransom, S., Roshi, A., Wagner, M., Werthimer, D., & Wharton, R. 2013, in *IAU Symposium*, Vol. 291, *IAU Symposium*, 57–57
- Spitler, L. G., Lee, K. J., Eatough, R. P., Kramer, M., Karuppusamy, R., Bassa, C. G., Cognard, I., Desvignes, G., Lyne, A. G., Stappers, B. W., Bower, G. C., Cordes, J. M., Champion, D. J., & Falcke, H. 2014, *ApJ*, 780, L3
- Tendulkar, S. P., Cameron, P. B., & Kulkarni, S. R. 2012, *ApJ*, 761, 76
- Thompson, C. & Duncan, R. C. 1993, *ApJ*, 408, 194
- Thompson, C., Lyutikov, M., & Kulkarni, S. R. 2002, *ApJ*, 574, 332
- van Langevelde, H. J., Frail, D. A., Cordes, J. M., & Diamond, P. J. 1992, *ApJ*, 396, 686
- Wex, N., Gil, J., & Sendyk, M. 1996, *A&A*, 311, 746
- Wharton, R. S., Chatterjee, S., Cordes, J. M., Deneva, J. S., & Lazio, T. J. W. 2012, *ApJ*, 753, 108
- Yelda, S., Ghez, A. M., Lu, J. R., Do, T., Meyer, L., Morris, M. R., & Matthews, K. 2014, *ApJ*, 783, 131
- Yusef-Zadeh, F., Roberts, D., Wardle, M., Heinke, C. O., & Bower, G. C. 2006, *ApJ*, 650, 189
- Zhang, F., Lu, Y., & Yu, Q. 2014, *ApJ*, 784, 106